AgRISTARS

SM-GO-04018
81-10158
TM 82002

A Joint Program for Agriculture and Resources Inventory Surveys Through Aerospace Remote Sensing

Soil Moisture

AUGUST 1980

NASA

Technical Memorandum 82002

CALCULATIONS OF THE SPECTRAL NATURE OF THE MICROWAVE EMISSION FROM SOILS

(E81-10158) CALCULATIONS OF THE SPECTRAL NATURE OF THE MICROWAVE EMISSION FROM SOILS (NASA) 66 p HC A04/MF A01 CSCL 08M

N81-24495

Unclas
G3/43 00158

T. Mo, T. J. Schmugge, and B. J. Choudhury

NASA

SM-GO-04018
TM-82002

CALCULATIONS OF THE SPECTRAL NATURE OF THE MICROWAVE EMISSION FROM SOILS

T. Mo[†]
T. J. Schmugge
B. J. Choudhury
Goddard Space Flight Center
Greenbelt, Maryland 20771

August 1980

[†]Computer Sciences Corporation, Silver Spring, MD 20910

CALCULATIONS OF THE SPECTRAL NATURE OF THE MICROWAVE EMISSION FROM SOILS

1. Introduction

There is considerable interest in the remote sensing of soil moisture content for a variety of disciplines (e.g., hydrology, meterology, and agriculture). A microwave radiometer is one of the most promising devices for detecting soil moisture because of its sensitivity to moisture and its ability to penetrate deep into the soil. At microwave frequencies, the dielectric constant of water is quite large, particularly the real part, which can have values up to 80, while that of dry soil is typically less than 5. Thus the water content of a soil can greatly affect its dielectric properties, which in turn, determine the propagation of electromagnetic waves in the soil media. Therefore, microwave radiometric observations will be sensitive to the water content in the soil.

Interpretation and analysis of microwave measurements require model calculations of the brightness temperature for a range of moisture and temperature profiles. Several radiative transfer models have been developed for such calculations (cf. Njoku and Kong, 1977, Choudhury, 1978; Burke, et al., 1979; Wilheit, 1978). Most of the models require detailed solutions of Maxwell's equations for electromagnetic waves propagating through stratified layers of the dielectric media. Accuracy of the calculations depends on the knowledge of the dielectric properties of layered soil media.

The radiative transfer model developed by Wilheit (1978) is particularly suited for calculating the brightness temperature from stratified layers of wet soils. A brief description of this model is given in Section 2. Wilheit's model

has been employed by several investigators (cf. Choudhury, et al., 1979; Choudhury, 1978; Mo and Choudhury, 1980; Schmugge and Choudhury, 1980) for studying the microwave emission from various soil conditions. Their results indicate the importance of surface conditions (smooth or rough) and soil moisture profile in determining the emission of the soil. Further simulations, which include extensive use of data obtained from field measurements, is necessary to better understand the relationships between soil moisture and brightness temperature. Calculations with ground truth data over an extensive period of time can show not only the diurnal variation of the brightness temperature but also the long-term trend as the moisture conditions vary within the soil. In this study, calculated results of brightness temperature, emissivity, effective temperature, moisture sampling depths, and other related microwave radiative quantities will be presented. The calculations were performed at the wavelengths of 2.8, 6, 11, 21, and 49 cm using the measured soil temperature and moisture profiles observed at the USDA facilities in Arizona and Georgia. An empirical model for the complex dielectric constant of mixed soil and water content (Wang and Schmugge, 1980) was employed. Calculated brightness temperature and emissivity are displayed as functions of the average soil moistures in four different soil depth intervals and statistically analyzed using a linear regression method. Correlation coefficients which measure the accuracy of the fit were also obtained.

2. RADIATIVE TRANSFER MODEL

The simulation model employed in the present study is based on the radiative transfer model developed by Wilheit (1978). This model is based on coherent radiation, and it is assumed that a general inhomogeneous ground with varying moisture can be stratified into N dielectric layers, each having a complex index of refraction n_j and thickness Δ_j. The last or bottom layer is semi-infinite. Electromagnetic waves can propagate in each layer. The electromagnetic waves in each layered dielectric medium are governed by Maxwell's equations (Jackson, 1962). Solutions of Maxwell's equations, with appropriate boundary conditions at the interfaces between layers, give the electric and magnetic fields in each layer. The electromagnetic energy flux entering a layer across a boundary is given by the Poynting vector $\vec{S}$. By conservation of energy, the electromagnetic energy falling on an interface is partially reflected; the other portion propagates through the layers and is partially absorbed. Each layer absorbs a fraction $f_j^p(\theta)$ of this energy, where j is an index specifying the layer, p denotes polarization and θ is the incident angle. This fraction $f_j^p(\theta)$ can be defined as (for simplicity, p and θ will be understood);

$$f_j = \frac{S_{j-1} - S_j}{S_1} \qquad (1)$$

where S_{j-1} is the net electromagnetic energy flux entering the jth layer at the (j-1)th interface, S_j the flux for the (j+1)th layer at the jth interface, and S_1 the flux incident on the first interface. If a layer j is in thermodynamic equilibrium at a constant temperature $T=T_j$, it must

also radiate as much energy as it absorbs. This blackbody radiation process is governed by Planck's law

$$B = \frac{2h\nu^3}{c^2}\left(\frac{1}{e^{h\nu/kT}-1}\right) \qquad (2)$$

where B is the power per unit area of radiator per unit band-width and per unit solid angle, h is Planck's constant, c the speed of light, and k Boltzman's constant.

In the microwave region, the Rayleigh-Jean approximation for Equation (2) can be used;

$$B = \frac{2\nu^2 kT}{c^2} \qquad (3)$$

The intensity B in Equation (3) is linearly proportional to the thermodynamic temperature T of the radiating layer. Therefore, an equivalent brightness temperature T_B can be defined by

$$T_B = \frac{Bc^2}{2\nu^2 k} \qquad (4)$$

This relation holds for each layer, since the amount of radiation from each layer is independent of the temperatures of other layers. Therefore, the resultant brightness temperature T_B of the soil can be represented by

$$T_B = RT_{sky} + \sum_{i=2}^{N} f_i T_i \qquad (5)$$

where R is the reflectivity for the incident sky radiation (in terms of the sky temperature T_{sky}) on the first interface, and T_i is the temperature of the ith layer. In the present study, sky radiation is excluded by ignoring the first term

in Equation (5), since its contribution is less than 5°K (typically $T_{sky} \approx 5°K$ and $R < 1$). By conservation of energy at the air-soil interface, the reflectivity R of the soil surface is

$$R \equiv 1 - \sum_{i=2}^{N} f_i = 1 - e \qquad (6)$$

where e is the effective emissivity. Equation (5) shows that calculation of the quantity f_i for each layer is the essential requirement to determine the brightness temperature from a general wet soil. The model developed by Wilheit (1978) gives a detailed description for calculating the quantity f_i as a function of index of refraction (or dielectric constant), incident angle, and wavelength.

A thermal radiative sampling depth δ_T, the characteristic soil depth where the upwelling thermal radiation originates, is defined by Wilheit (1978) as

$$\delta_T = \frac{\sum_{i=2}^{N} x_i f_i}{\sum_{i=2}^{N} f_i} \qquad (7)$$

where x_i is the depth of the ith layer. The quantity δ_T is determined by the imaginary part of the index of refraction. For a uniform dielectric media, Equation (7) reduces to

$$\delta_T = \frac{\lambda}{4\pi \ \mathrm{Im}(n)} \qquad (8)$$

where n is index of refraction and λ is the free space wavelength of the radiation.

Another related radiation quantity is the reflectivity sampling depth δ_r, which Wilheit defined as the soil depth over which the reflectivity would result from an index of refraction n changed from $n_o = 1$ (air) to $(n_1 + n_2)/2$, where n_1 is the refractive index at the surface of the soil, and n_2 corresponds to the refractive index at the soil depth to which a wave can penetrate. This representation has been described by Wilheit (1978) as shown schematically in Figure 1. The refractive index changes from n_o (corresponding to air) to n_1 at the air-soil interface, then varies linearly with depth from n_1 to n_2 at a depth of $\delta = 2\delta_r$. The reflectivity sampling depth δ_r is wavelength-dependent and the ratio δ_r/λ is in the range 0.032 to 0.073 (Wilheit, 1978).

The change in n ($=\sqrt{\varepsilon}$, where ε is the soil dielectric constant) over the transition region δ is primarily caused by the moisture variation in the soil. The thickness δ is an estimate of the thickness of the soil layer whose moisture content determines the surface emissivity. Therefore, δ is called the moisture sampling depth, and its value will be estimated from the calculated emissivities and the moisture profiles in Section 5. The procedure for estimating δ will be to compare the calculated emissivity with that determined for a uniform profile using the Fresnel equations. The moisture content of this uniform profile will define an effective soil moisture (SM_{eff}). The varying profile soil moisture will be integrated over layers of different thickness until a value equal to SM_{eff} is obtained; the thickness of this layer will be an estimate of δ.

In the present study, the brightness temperature T_B, the thermal and moisture sampling depths, δ_T and δ, respectively are investigated using a large data base of ground temperature and moisture profiles measured in Arizona and Georgia.

Another parameter of interest is the effective soil temperature over the thermal sampling depth given by

$$T_e = \frac{\sum_{2}^{N} f_i T_i}{\sum_{2}^{N} f_i} \qquad (9)$$

where T_i is the physical temperature of the ith layer.

The surface emissivity e for a general inhomogeneous wet soil is defined as the ratio

$$e = \frac{T_B}{T_e} = 1 - R \qquad (10)$$

if Equations (5), (6), and (9) are employed (with $T_{sky} = 0$). The quantity e was also computed in this study. Relationships of e and the soil moistures within four different soil depth intervals were explored in the present work.

3. EMPIRICAL MODEL OF DIELECTIRC CONSTANT FOR WET SOILS

An empirical model for the complex dielectric constant of soils as a function of moisture content was recently developed by Wang and Schmugge (1980) who expressed the dielectric constant of a soil-water mixture in terms of the direct mixing of the dielectric constants of the constituents.

The model is based on the fact that the initially absorbed water does not behave as free water due to its binding or proximity to the soil particle surface. This binding inhibits the polarizability of these water molecules.

As a result, there is a slow increase of the soils dielectric constant with soil moisture below a transition moisture W_t; above this level, there is a much more rapid increase in dielectric constant. W_t is a function of the soil's texture and has been found to be linearly related to its wilting point (WP). Dielectric constant measurements for a number of soils were used by Wang and Schmugge (1980) to obtain the following expressions,

$$\varepsilon = W_c \varepsilon_x + (P - W_c)\, \varepsilon_a + (1 - P)\varepsilon_r, \quad W_c \leq W_t \tag{11}$$

with

$$\varepsilon_x = \varepsilon_i + (\varepsilon_w - \varepsilon_i)\frac{W_c}{W_t}\gamma \tag{12}$$

and

$$\varepsilon = W_t \varepsilon_x + (W_c - W_t)\varepsilon_w + (P - W_c)\varepsilon_a + (1 - P)\varepsilon_r, \quad W_c > W_t \tag{13}$$

with

$$\varepsilon_x = \varepsilon_i + (\varepsilon_w - \varepsilon_i)\gamma \qquad (14)$$

where P is the porosity of the dry soil; ε_a, ε_w, ε_r and ε_i are the dielectric constants of air, water, rock, and ice, respectively. The ε_x stands for dielectric constant of the initially absorbed water. W_c is the volumetric water content (in cm^3/cm^3, cubic centimeter of water per cubic centimeter of dry soil medium) and W_t is the transition moisture, which divides the dielectric constant of soil into two different segments as a function of moisture content, as defined by Equations (11) and (13).

The dielectric constant of a soil increases slowly as a function of soil moisture when W_c is less than W_t, but it will increase steeply once W_c becomes greater than W_t. The W_t can be represented by (Wang and Schmugge, 1980).

$$W_t = 0.49\ WP + 0.165 \qquad (15)$$

The wilting point WP (in cm^3/cm^3), defined as the soil moisture at which the release of water to a plant is too small to counterbalance the transpiration losses, is given by

$$WP = 0.06774 - 0.00064\ Sand + 0.00478\ Clay \qquad (16)$$

Sand and Clay are the amounts (in percent) of sand and clay in the soil. The parameter γ in Equations (12) and (14) is defined by

$$\gamma = -0.57\ WP + 0.481 \qquad (17)$$

Each of the dielectric constants ε in the above equations consists of real and imaginery parts (i.e., $\varepsilon = \varepsilon_R + i\varepsilon_I$). The dielectric constants used in the calculation for ice, air, rock, and water are given in Table 1. The other parameter values used in the present work are: P = 0.5, Sand = 32%, and Clay = 22%.

The dielectric constant is a function of wavelength (or frequency). The values of dielectric constants for the soil constituents (i.e., ice, air, rock, and water) used in the present work are listed in Table 1. The wavelength-dependence of ε for ice, air, and rock is ignored because its effect is relatively small in comparison to that of water. The dielectric constant, ε_w, of water varies rapidly as the wavelength λ changes from 2.8 to 49 cm (as shown in Table 1). The values of ε_w were calculated with an empirical formula (Wang and Schmugge, 1980) at an assumed temperature of 293°K. The dielectric constant of a medium also depends on temperature; however, this temperature effect can be ignored if the variation in temperature is not very large.

The dielectric constant for the soil used here as a function of soil moisture, W_c, is shown in Figure 2. The real and imaginary parts of the dielectric constant of soil shown in Figure 2 were calculated according to Equations (11) and (13) at the wavelengths of 2.8 and 21 cm, respectively. It is important to note the large decrease in the imaginary part of the dielectric constant as the wavelength increases from 2.8 to 21 cm. According to Equation (8), a decrease in the imaginary part of the dielectric constant will cause an increase in the thermal sampling depth δ_T.

Table 1

The values of real and imaginary parts of dielectric constants for ice, air, rock, and water used in the present work.

ε	Real Part*	Imaginary Part*	Remark
ε_i	3.2	0.1	Ice
ε_a	1.0	0.0	Air
ε_r	5.5	0.2	Rock
ε_w	56.4	34.9	λ = 2.8 cm
	73.3	21.7	6.0 cm
	77.9	12.6	11 cm
	79.5	6.6	21 cm
	80.0	2.9	49 cm

*These values correspond to a temperature of 293°K.

The emissivity corresponding to the dielectric constant of soil shown in Figure 2 can be calculated with the Fresnel formula for a homogenous medium (cf. Schmugge and Choudhury, 1980). For perpendicular incidence, the Fresnel emissivity for a smooth surface is given by

$$e = 1 - \left| \frac{\sqrt{\varepsilon} - 1}{\sqrt{\varepsilon} + 1} \right|^2 \qquad (18)$$

where ε is the dielectric constant of soil.

Figure 3 shows the Fresnel emissivity calculated as a function of soil moisture at $\lambda = 21$ cm using the soil dielectric constant shown in the upper part of Figure 2. This calculated emissivity curve (Figure 3) and similar ones at other wavelengths will be used to estimate soil moisture sampling depths in Section 5.

4. MOISTURE AND TEMPERATURE PROFILES

Two sets of field-measured data of soil moisture and temperature profiles provide the basis for our model calculation of brightness temperature and related quantities of microwave emission. The Arizona data were described by Jackson (1973) of the U. S. Water Conservation Laboratory (USWCL). These USWCL data were taken from irrigated soils at half hour intervals for a period of 15 days, from March 5 through March 18, and again on March 25, 1971. For each measurement the temperature profiles were taken at 13 depths, ranging from 0.1 to 128 cm, while soil moisture measurements were obtained for 16 depth intervals. Table 2 gives the depths of these temperature measurements and the intervals of the soil moisture profiles. The Georgia data were taken by Bruce, et al., (1977) at the USDA Southern Piedmont Conservation Research Center, from June 15 to June 23, 1973, at 45-minute intervals. Each profile of the Georgia data contains 10 values of soil moisture and 9 temperatures at the depths listed in Table 2.

From each of these measured data sets, a six-point polynomial interpolation procedure was used to create a new set of moisture or temperature profiles which were used to determine the moisture and temperature values of the stratified soil layers as required for the model calculation.

Table 2

The ground soil depths and intervals at which the temperatures and water contents were measured in Arizona and Georgia, respectively

Layer	Depth of Temperature Measurement (cm)		Depth Interval of Water Measurement (cm)	
	Arizona	Georgia	Arizona	Georgia
1	0.1	0	0-0.5	0-0.5
2	0.5	0.5	0-1	.5-1.0
3	.75	1	1-3	1-2
4	1	3	3-5	2-3
5	2	7	5-9	3-4
6	3	15	9-10	4-5
7	4	30	10-15	5-7
8	5	60	15-20	7-9
9	8	120	20-30	9-12
10	16		30-40	12-15
11	32		40-50	
12	64		50-60	
13	128		60-70	
14			70-80	
15			80-90	
16			90-100	

5. RESULTS

Brightness temperatures, emissivities and effective temperatures were calculated at the five wavelengths of 2.8, 6, 11, 21, and 49 cm, using the ground temperature and moisture profiles measured in Arizona and Georgia. Figure 4 shows some typical results of the brightness temperature at the 21 cm wavelength calculated with the Arizona data of 8 selected days.

The curves in Figure 4 demonstrate diurnal variation and long-term pattern of changes within this period. Each curve in Figure 4 has a maximum around 4 p.m. and a minimum around 7 a.m. This diurnal variation of T_B is due to the large variation in near surface soil moistures. The minimum value of surface soil moisture during the day usually occured around 4 p.m., which coincides with the time of maximum brightness temperature. The diurnal variation is most pronounced on March 5, and gradually decreases from one day to the next as the soil dries.

Figure 4 also shows that as the soil moisture gradually decreases from March 5 to 25, the calculated brightness temperature increases from about 175°K to 265°K at midnight, an increase of 90°K.

Figure 5 shows the relationships among the effective temperature T_e (denoted by the solid curves on the upper parts), the surface temperature, T_s (the asterisk curves), and the emissivity (labeled by E on the ordinates at the lower parts). All the quantities shown in Figure 5 are obtained with the Arizona data, and the corresponding results obtained with the Georgia data are shown in Figure 6. The origin of the abscissa (time axis) corresponds to the 0th hour of March 5, 1971, and the time increases through March 18; the last 24-hour period in Figure 5 corresponds

to March 25, 1971; this 7-day gap in the measured data produces the small discontinuities at the 336th hour in Figure 5. At the 2.8 cm wavelength, T_e tracks the surface temperature very closely when wet; this indicates that the temperature sampling depth (δ_T) is approximately the same as the surface temperature measurement depth, i.e., 0.1 cm. For the 49 cm wavelength there is only a 2° or 3°K diurnal variation of T_e and only about a 5°K change in the daily average value of T_e. This difference results not only from the increased wavelength, but also the imaginary part of the dielectric constant for water which is much larger at 2.8 cm than at 49 cm.

The curves in Figure 5 show that the emissivity of wet soils (left hand side of the figure) has large diurnal variations, while that of dry soils (right hand side) has very little diurnal variation. Since the emissivity is defined as the ratio of the brightness temperatue (T_B) to T_e, a constant value of emissivity implies that the brightness temperature has the same pattern of diurnal variation as that of T_e, as seen in the right hand parts of the curves in Figure 5. The magnitudes of emissivity and T_e gradually decrease as the wavelength increases from 2.8 cm to 49 cm, and the diurnal variation for both quantities also becomes less pronounced at the longer wavelengths. These spectral dependences of emissivity and T_e are consistent with the fact that longer wavelength radiation can penetrate through deeper soil depths, where the moisture and temperature have smaller diurnal variations. Calculated results at λ = 49 cm show particularly small diurnal variation in T_e, even during the wet period as shown in the lowest part in Figure 5.

Figure 6 shows the results for emissivity, surface and effective temperatures, using the Georgia data of soil moisture and temperature profiles. The origin of the abscissa in Figure 6 corresponds to 7 p.m., June 15, 1973. The sudden drops in the emissivity around the 114th and 132th hour in Figure 6 were caused by two rains of 0.97 cm and 0.41 cm, respectively. It is interesting to note that the magnitude of the 49 cm emissivity during the rainfall period is larger than those of other wavelengths. This is due to the fact that the soil moistures have 'V-shaped' or inverted profiles during the rainfall period (shown in Figure 14 by the profile marked by 21) and the minimum in these moisture profiles is located at a depth of 1-2 cm. The emissivity at 49 cm wavelength is determined by the average moisture in a thicker layer at the surface. Thus, dry soil beneath the surface wet layer serves to increase the emissivity at the 49 cm wavelength compared to the emissivities at the shorter wavelengths.

Figure 5 shows that the T_e values calculated at $\lambda = 2.8$ cm are almost equal to the observed soil surface temperatures when the soils are wet. However, differences between the two quantities T_e and T_s gradually appear as the soil becomes dry, or the wavelength becomes longer. Plots of calculated effective temperatures versus observed soil surface temperatures (from the Arizona data) are given in Figure 7 for five different wavelengths, as labeled on each plot, respectively.

Figure 7 shows that T_e values at short wavelengths are linearly proportional to the surface temperatures, particularly at $\lambda = 2.8$ cm, except at the high surface temperature region where slight deviation from the linear relationship exists. As the wavelength increases, this linear relationship

gradually disappears. At λ = 49 cm, the effective temperature approaches, approximately, a constant value centered around 289°K, corresponding to a deep layer soil temperature. It is shown in another report (Choudhury, et al., 1980) that the effective temperature can be adequately parameterized as a function of two soil temperatures, one corresponding to the surface and another to a deep soil layer.

Calculated brightness temperature and emissivity at the wavelengths of 2.8, 6, 11, 21, and 49 cm, using the ground truth data observed in Arizona and Georgia, are displayed in Figures 8-11 as function of soil moistures within the four soil depth intervals, 0-2, 0-5, 0-9, and 0-15 cm, respectively. Figures 8a - 8e show the brightness temperatures calculated with the Arizona data at five wavelengths, and Figures 9a - 9e display the corresponding emissivities. A total of 720 values of brightness temperature (or emissivity), corresponding to the number of soil profiles measured in Arizona, were used in these computer generated plots. Figures 10 and 11 show the calculated brightness temperature and emissivity using the soil profiles from the Georgia data. The plots in Figures 8-11 show that the brightness temperature and emissivity vary almost linearly as a function of soil moisture. Conversely, the soil moisture is also a linear function of brightness temperature or emissivity and can be parameterized by the simple relation.

$$y_i = A + BX_i \qquad (19)$$

where y_i represents the moisture within the ith depth interval, X_i is either brightness temperatue or emissivity, and A and B are two adjustable parameters (regression coefficients).

The emissivities shown in Figures 9 and 11 remain constant when the soil moisture is small. These constant emissivities and the corresponding brightness temperatures at all wavelengths were excluded in the linear regression. This exclusion eliminates those results with e greater than 0.89 in the Arizona data, (and e greater than 0.90 in the Georgia data) from the linear regression analysis, and it produces correlation coefficients which are higher than those without exclusion. For example, when all brightness temperatures are included, the correlation coefficient $r = -0.8411$ (at $\lambda = 21$ cm) is obtained in the linear regression of T_B with the soil moistures in the top 5 cm soils from the Arizona data, while $r = -0.9032$ if brightness temperatures corresponding to e greater than 0.89 are excluded.

A least-square procedure was employed to obtain the values of A and B for the cases shown in Figures 8-11. The best-fit values of A and B from the Arizona data are listed in Table 3 for the brightness temperatue and emissivity. Correlation coefficients r are also given in Table 3. The corresponding results from the Georgia data are given in Table 4. The quantities SM1, SM2, SM3, and SM4 (listed in Tables 3 and 4) represent the soil moistures within the depth intervals of 0-2, 0-5, 0-9, and 0-15 cm, respectively. The correlation coefficients in Tables 3 and 4 show that SM1 has the best correlation with the calculated brightness temperature and emissivity, and that, with the exception of the 49 cm case, the correlation is higher for the emissivity. The correlation coefficient decreases for moisture in deeper depth. However, Table 3 shows that some of the correlation coefficients at SM3 and SM4 are larger than those at SM2.

Table 3

Best-fit parameters and correlation coefficients for the Arizona data.

λ (cm)	PARAMETER	EMISSIVITY				BRIGHTNESS TEMPERATURE			
		SM1	SM2	SM3	SM4	SM1	SM2	SM3	SM4
2.8	A	0.7309	0.5048	0.5065	0.4904	0.7318	0.4937	0.5062	0.4961
	B	-0.6357	-0.3089	-0.3179	-0.2863	-2.261E-03	-1.046E-03	-1.127E-03	-1.043E-03
	r	-0.9599	-0.9301	-0.9370	-0.9273	-0.8925	-0.9086	-0.8739	-0.8420
6.0	A	0.7060	0.4889	0.4910	0.4800	0.6911	0.4752	0.4858	0.4787
	B	-0.6158	-0.2929	-0.3027	-0.2778	-2.108E-03	-9.723E-04	-1.046E-03	-9.758E-04
	r	-0.9666	-0.9176	-0.9306	-0.9294	-0.9130	-0.8935	-0.8710	-0.8555
11	A	0.6746	0.4843	0.4777	0.4645	0.6557	0.4711	0.4701	0.4604
	B	-0.5739	-0.2873	-0.2850	-0.2571	-1.937E-03	-9.523E-04	-9.701E-04	-8.878E-04
	r	-0.9791	-0.9159	-0.9412	0.9429	-0.9492	-0.9040	-0.9047	-0.8935
21	A	0.9009	0.5669	0.5380	0.5417	0.8429	0.5480	0.5173	0.5211
	B	-0.9091	-0.4038	-0.3783	-0.3732	-2.914E-03	-1.324E-03	-1.228E-03	-1.210E-03
	r	-0.9931	-0.9250	-0.9892	-0.9788	-0.9918	-0.9032	-0.9758	-0.9664
49	A	1.0460	0.7225	0.6038	0.5907	1.0017	0.7002	0.5866	0.5742
	B	-1.1511	-0.6342	-0.4865	-0.4580	-3.794E-03	-2.099E-03	-1.610E-03	-1.514E-03
	r	-0.9935	-0.9227	0.9915	-0.9868	-0.9957	-0.9206	-0.9894	-0.9857

Table 4

Best-fit parameters and correlation coefficients for the Georgia data.

λ (cm)	PARAMETER	EMISSIVITY				BRIGHTNESS TEMPERATURE			
		SM1	SM2	SM3	SM4	SM1	SM2	SM3	SM4
2.8	A	0.5275	0.4059	0.3917	0.3896	0.5318	0.4097	0.3945	0.3993
	B	-0.4916	-0.3319	-0.2810	-0.2408	-1.665E-03	-1.127E-03	-9.526E-04	-8.487E-04
	r	-0.9688	-0.9030	-0.8260	-0.7201	-0.9587	-0.8906	-0.8330	-0.6845
6.0	A	0.5016	0.3830	0.3690	0.3678	0.5069	0.3870	0.3720	0.3749
	B	-0.4646	-0.3059	-0.2541	-0.2143	-1.581E-03	-1.043E-03	-8.649E-04	-7.493E-04
	r	-0.9676	-0.9083	-0.8519	-0.7323	-0.9603	-0.8997	-0.8451	-0.7070
11	A	0.4776	0.3679	0.3575	0.3611	0.4785	0.3688	0.3580	0.3643
	B	-0.4392	-0.2902	-0.2428	-0.2087	-1.476E-03	-9.769E-04	-8.163E-04	-7.138E-04
	r	-0.9758	-0.9268	-0.8726	-0.7362	-0.9719	-0.9215	-0.8687	-0.7203
21	A	0.5771	0.4139	0.3839	0.3842	0.5684	0.4090	0.3797	0.3801
	B	-0.5498	-0.3358	-0.2649	-0.2273	-1.812E-03	-1.108E-03	-8.730E-04	-7.467E-04
	r	-0.9718	-0.9179	-0.8969	-0.7468	-0.9750	-0.9196	-0.8998	-0.7515
49	A	1.3848	0.7471	0.5838	0.5765	1.3096	0.7213	0.5678	0.5638
	B	-1.5101	-0.7271	-0.4955	-0.4492	-4.747E-03	-2.326E-03	-1.592E-03	-1.450E-03
	r	-0.8979	-0.9453	-0.9325	-0.8076	-0.8992	-0.9302	-0.9139	-0.7878

This can be understood from the scatter plots in Figures 8 and 9 which show that there are more scattered points in the soil moisture region 0.1-0.2 for the SM2 case than those for SM3 or SM4, i.e., there were not many profiles that were dry enough through the top 9 or 15 cm.

The soil moisture within the 5 depth intervals, 0-2, 0-5, 0-9, 0-15, and 0-25 cm, is shown in Figure 12 as a function time. The first four of these average soil moistures are used to produce the plots in Figures 8 and 9. Figure 12 shows that large diurnal variations in the soil moisture exists in the top layers, and there is only gradual decrease in the cases of 0-15 and 0-25 cm.

Soil brightness temperature represents the microwave energy emitted from some soil volume; it is important to know the thermal sampling depths, from which radiation originated. This is defined in Equation (7). Figure 13 shows that at 21 cm wavelength, this depth varies from 11 cm for wet conditions (March 5) to 20 cm for dry day (March 25). These 21-cm values of thermal sampling depth agree with the results of 5 to 25 cm given by Blanchard and Bausch (1979). Newton (1977) found that the sampling depth sensed by the L-band is linearly related to the average moisture in the profile.

The thermal sampling depth is wavelength-dependent; according to Equation (8), it is directly proportional to wavelength for a uniform medium, besides depending on the imaginary part of the index of refraction. Calculations show that the thermal sampling depths for λ = 2.8 cm (X-band) are in the range of 0.2 to 2 cm, which is about 10 to 20 times smaller than those at 21 cm.

Thermal sampling depths at other wavelengths are about one wavelength in dry soil and a few tenths of a wavelength in wet soil.

The soil moisture sampling depth δ has been discussed in Section 2. The magnitude of δ for each soil moisture profile used in the present study can be estimated by comparing the emissivity obtained from the Wilheit model with that from the Fresnel method as defined in Equation (18). The process assumes that the Fresnel emissivity function as shown in Figure 3, and similar ones at other wavelengths, are taken as 'standard' functional forms relating emissivity and soil moisture. Assuming the model calculated emissivity is identical to that of the Fresnel method, one can obtain a Fresnel moisture SM_f from the intersection of the model calculated emissivity with the Fresnel curve (such as shown in Figure 3). This Fresnel moisture SM_f corresponds to an average soil moisture within a soil depth interval δ, the moisture sampling depth as shown in Figure 1. This moisture sampling depth δ for each soil moisture profile used in the present work was determined from the illustration in Figure 14a. The solid curves in Figure 14a are four soil moisture profiles measured in Arizona (Jackson, 1973). The value of δ is obtained from the integrated soil moisture in a soil layer of thickness δ (as shown by the shaded area in Figure 14a) which satisfies the relation,

$$SM_f = \frac{1}{\delta} \int_0^{\delta} SM(x)\,dx \qquad (20)$$

where $SM(x)$ is the soil moisture at the soil depth x. Equation (20) shows that δ can be numerically obtained if the quantities SM_f and the moisture profile are known.

A computer program was developed to perform the numerical integration of Equation (20), and the calculation procedures outlined in the following steps: (1) For each model calculated emissivity, the value of SM_f is obtained from the Fresnel emissivity curve (such as shown in Figure 3) using a six-point polynominal interpolation subroutine, (2) values of SM(x) along the moisture profiles are interpolated in steps of $\Delta x = 0.1$ cm with the six-point polynominal interpolation subroutine, and (3) the trapezoidal rule is employed to perform the integration in Equation (20) up to a thickness δ such that the expression on the right hand side of Equation (20) produces an average soil moisture equal to SM_f. This thickness δ, thus determined, is the desired moisture sampling depth.

Figures 15 and 16 show some of the calculated moisture sampling depths as functions of diurnal times for 3 days and five different wavelenghts. The moisture profiles used in these calculations are taken from the Arizona data measured in March 1971. The soil conditions were wet on March 7, moist on March 9, and dry on March 18. The results for all 3 days are shown for the 21- and 49-cm wavelengths in Figure 16. At the wavelengths of 6 and 11 cm, the moisture sampling depths for the dry soils of March 18 are essentially zero, therefore they are not shown in Figure 15. In the 2.8-cm case, only the results for the wet soils of March 7 are given in Figure 15, since those for the other days are too small to display.

The calculated moisture sampling depths in Figures 15 and 16 show large diurnal variations, particularly at the longer wavelengths of 21 and 49 cm. The striking features of the plots in Figure 16 are the large peaks occuring in the early afternoons and the low moisture sampling depths at night. These diurnal variations in the moisture

sampling depth are caused primarily by the changes in the soil moisture profiles, corresponding to the surface of the soil being dried by evaporation in the daytime and moistened by condensation at night. The soil moisture profiles are quite uniform in the nighttime and thus, only a small thickness δ is required to produce an average soil moisture SM_f, as defined in Equation (20). By contrast, the daytime moisture profiles usually have very dry surface layers and steep gradient variations as a function of depth, particularly in the early afternoons; the peak values of the moisture sampling depth result from these moisture profile variations.

It has been shown that emissivities calculated with coherent radiative transfer models (such as the one used in the present study) have resonance behavior at certain moisture sampling depths (see Schmugge, et al, 1974; and Wilheit, 1978). Any resonance in the model calculated emissivity values would produce uncertainty in the corresponding moisture sampling depths as shown in Figures 15 and 16. The effect of this emissivity resonance can be reduced (or eliminated) by increasing the imaginary part of complex soil dielectric constant in the model calculation. To investigate this resonance effect, we repeat our emissivity and moisture-sampling-depth calculations using ε_r = (5.5, 2.0) for the dielectric constant of rock, instead of that given in Table 1. The resulting moisture sampling depths are shown in Figures 17 and 18, which should be compared with Figures 15 and 16, respectively. Comparison of the results in Figures 15 and 16 with the corresponding ones in Figures 17 and 18 shows that the moisture sampling depths obtained from calculations with the larger ε_r = (5.5, 2.0) value are generally greater than those from the normal ε_r = (5.5, 0.2). The variation depends on wavelength and

time of day, e.g., at λ = 21 cm, the peak values in the moisture sampling depth in Figure 18 are greater than the corresponding ones in Figure 16 by 24 percent for March 7, 19 percent for March 9, and 54 percent for March 18.

The peak values for moisture sampling depths in Figures 15-18 are in the range 0.06λ to 0.1λ which agrees well with previously calculated results (Schmugge et al., 1974 and Wilheit, 1978).

6. SUMMARY AND DISCUSSION

We have calculated the microwave radiative quantities of brightness temperature, effective temperature, thermal sampling depth, reflective or soil moisture sampling depth, and emissivity for a set of soil profiles observed at the USDA facilities in Arizona and Georgia. All calculations were performed at the wavelengths of 2.8, 6, 11, 21, and 49 cm, using a coherent radiative transfer model developed by Wilheit (1978). Calculated values of emissivity show strong diurnal variations when the soils are wet, while there is only a small diurnal change when the soil is dry.

The effective temperatures corresponding to wet soils are approximately equal to the soil surface temperatures at the short wavelength of λ = 2.8 cm, while large differences between the two quantities appear at longer wavelengths or at dry soil condition.

The thermal sampling depth is found to be a function of wavelength and soil condition. Calculations show that the thermal sampling depth is approximately one wavelength in dry soil and gradually decreases to about 0.1-0.5 wavelength in wet soil.

The soil moisture sampling depth, which is smaller than the thermal sampling depth, also depends on wavelength, and are in the order of 0.06λ to 0.1λ. The moisture sampling depths represent the thickness of the soil layer which contains an average amount of soil moisture having a large effect on the emissivity of the soil. Some estimated values of moisture sampling depth for three selected days are given in Figures 15 and 16.

Uncertainties in the measured soil-moisture profiles also affect the calculated results. Investigations of these

uncertainties and the effect of surface roughness on the emissivity and brightness temperature will be described elsewhere.

Acknowledgements: We wish to thank Dr. Leslie H. Gesell of Computer Sciences Corporation for reading the manuscript.

References

Blanchard, B. J., and W. Bausch, 1979: Algorithms to Estimate Soil Moisture Storage From Microwave Measurements, TR-RSC-3843, Remote Sensing Center, Texas A&M University, College Station, Texas 77843.

Bruce, R. R., A. W. Thomas, L. A. Harper, and R. A. Leonard, 1977: Diurnal soil water regime in the tilled plow layer of a warm humid climate, Soil Sci. Soc. Amer. J., 41, 455-460.

Burke, W. J., T. Schmugge, and J. F. Paris, 1979: Comparison of 2.8 and 21 cm Microwave Radiometer Observations over Soils with Emission Model Calculations, J. Geophys. Res., 84, pp. 287-294.

Choudhury, B. J., 1978: A Radiative Transfer Model for Microwave Emission From Soils, Computer Sciences Corporation, Silver Spring, Maryland, TM-78-6001.

Choudhury, B. J., T. J. Schmugge, and T. Mo, 1980: A Parameterization of Effective Soil Temperature for Microwave Emission (in preparation).

Choudhury, B. J., T. J. Schmugge, R. W. Newton, and A. Chang, 1979: Effect of Surface Roughness on the Microwave Emission from Soils, J. Geophys. Res., 84, pp. 5699-5706.

Jackson, J. D., 1962: Classical Electrodynamics, John Wiley, New York.

Jackson, R. D., 1973: Diruanl Soil-Water Content Changes during Drying, Field Solar Water Regime, SSSA Spec. Publ. 5, pp. 37-56, Soil Sci. Soc. of Amer. Madison, Wisconsin.

Mo, T., and B. J. Choudhury, 1980: Diurnal Variation of Microwave Brightness Temperature of Soils, Technical Report, CSC/TR-80/6003, Computer Sciences Corporation, Silver Spring, Maryland.

Newton, R. W., 1977: Microwave Remote Sensing and Its Application to Soil Moisture Determination, Technical Report RSC-81, Remote Sensing Center at Texas A&M University, College Station, Texas 77843.

Njoku, E. G., and J. A. Kong, 1977: Theory for Passive Microwave Sensing of Near-Surface Soil Moisture, J. Geophys. Res., 82, pp. 3108-3118.

Schmugge, T. J., and B. J. Choudhury, 1980: A Comparison of Radiative Transfer Models for Predicting the Microwave Emission from Soils, Technical Memorandum 80688, NASA Goddard Space Flight Center, Greenbelt, Maryland 20771.

Schmugge, T. J., P. Gloersen, T. Wilheit, and F. Geiger, 1974: Remote Sensing of Soil Moisture with Microwave Radiometers, J. Geophys. Res., 79, pp. 317-323.

Wang, J. R., and T. J. Schmugge, 1980: An Empirical Model for the Complex Dielectric Permittivity of Soils as a Function of Water Content, IEEE Trans. Geosci. and Remote Sensing, GE-18, pp. 288-295.

Wilheit, T. T., 1978: Radiative Transfer in a Plane Stratified Dielectric, IEEE Trans. Geo. Electron., GE-16, pp. 138-143.

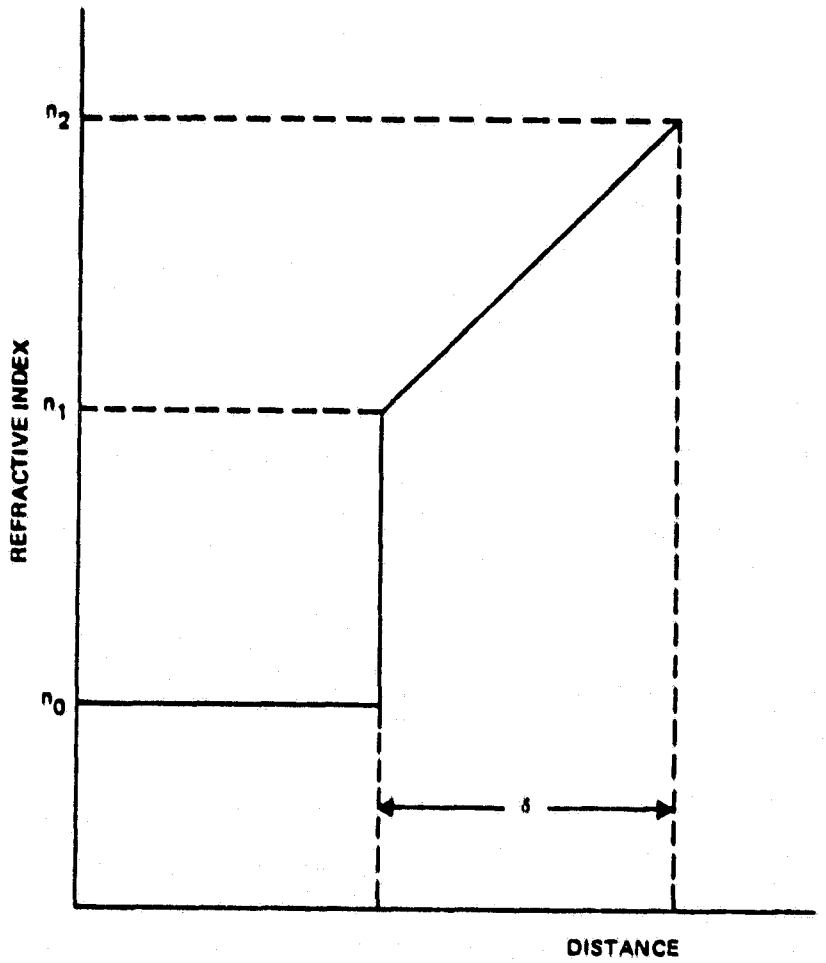

Figure 1. Schematic illustration of variation of index of refraction at the air-to-soil interface.

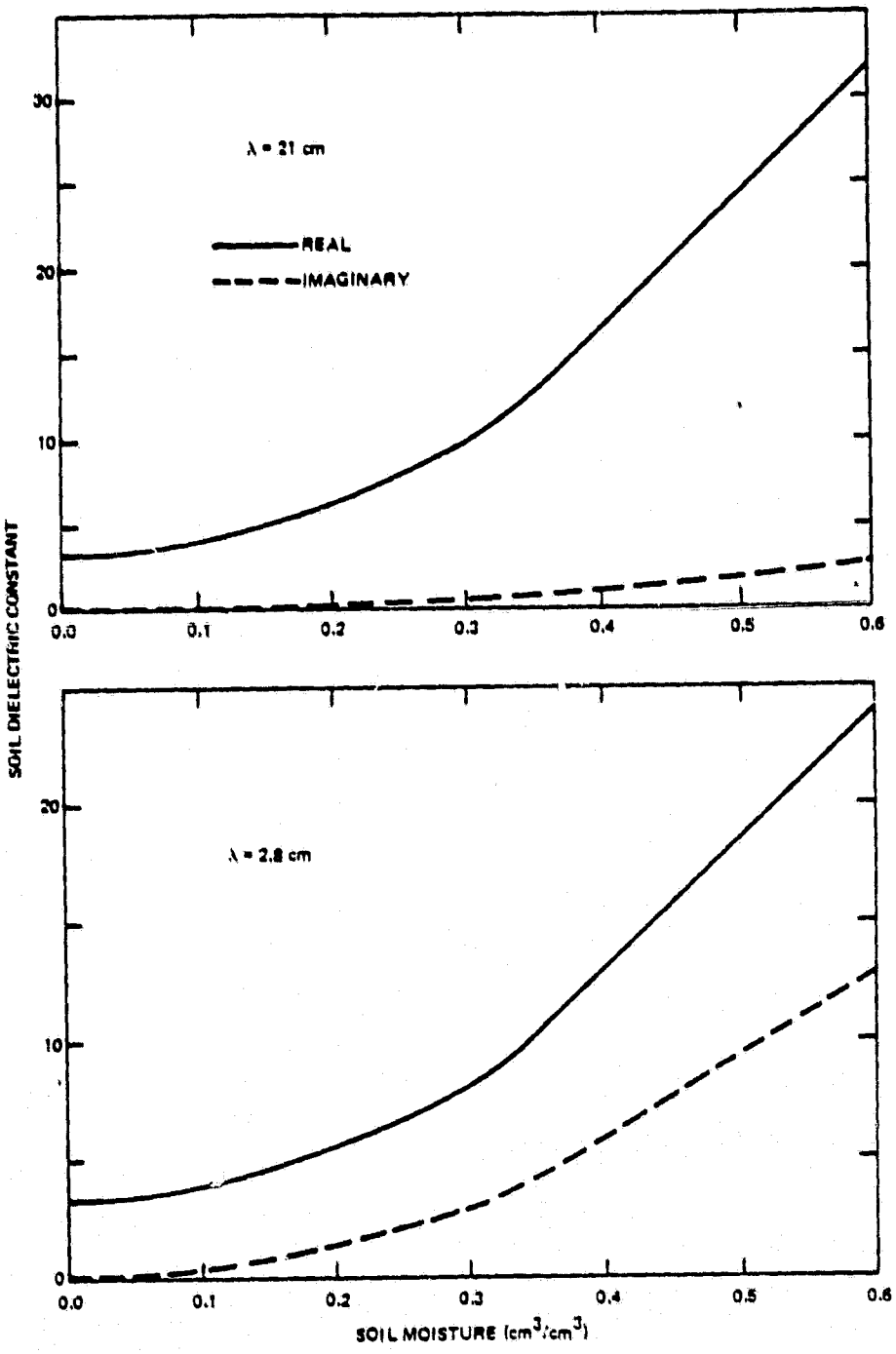

Figure 2. Real and imaginary parts of dielectric constant of soils at the wavelengths of λ = 2.8 cm and 21 cm.

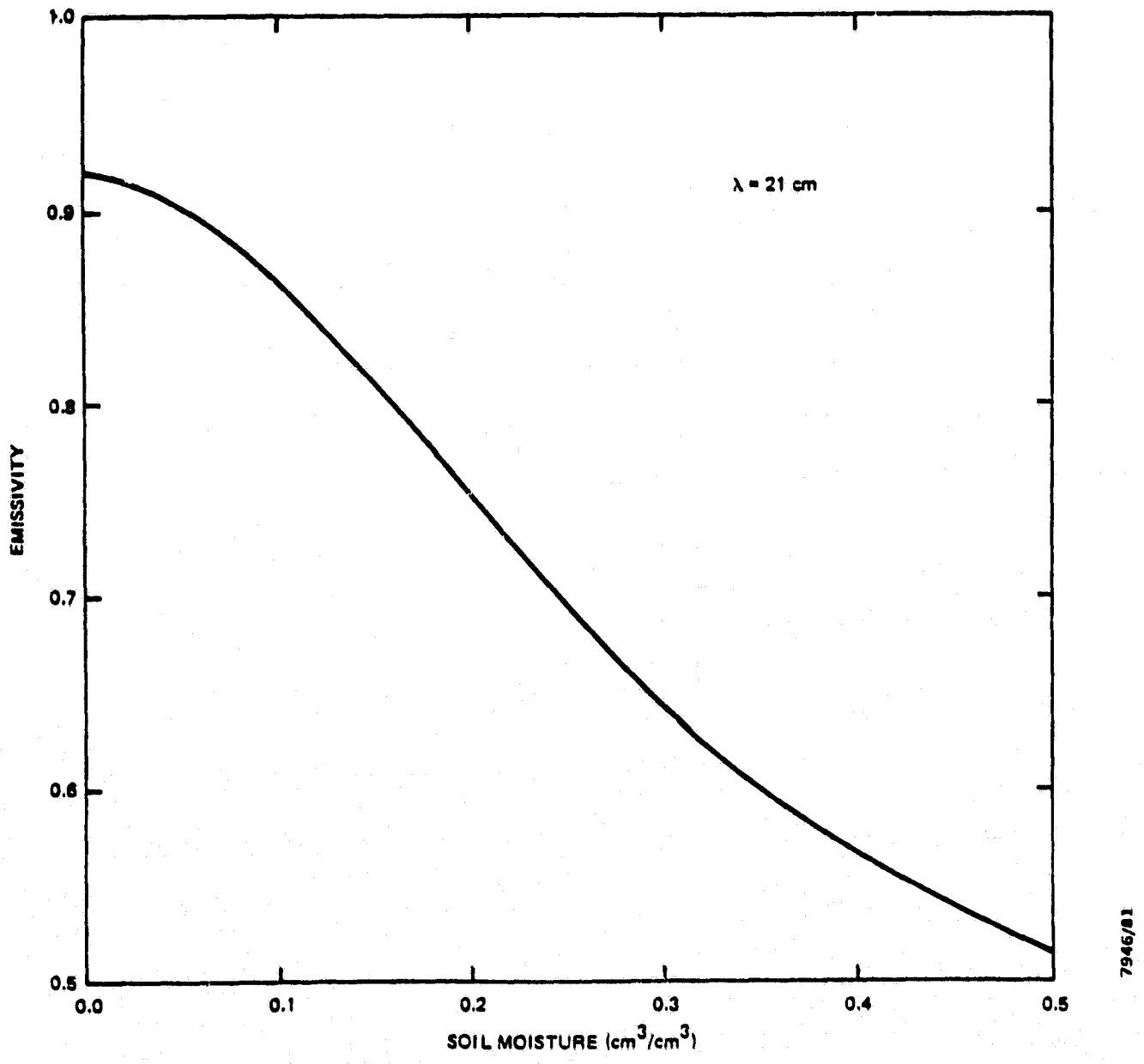

Figure 3. Calculated emissivity at λ = 21 cm using Fresnel formula and the dielectric constant given in Figure 2.

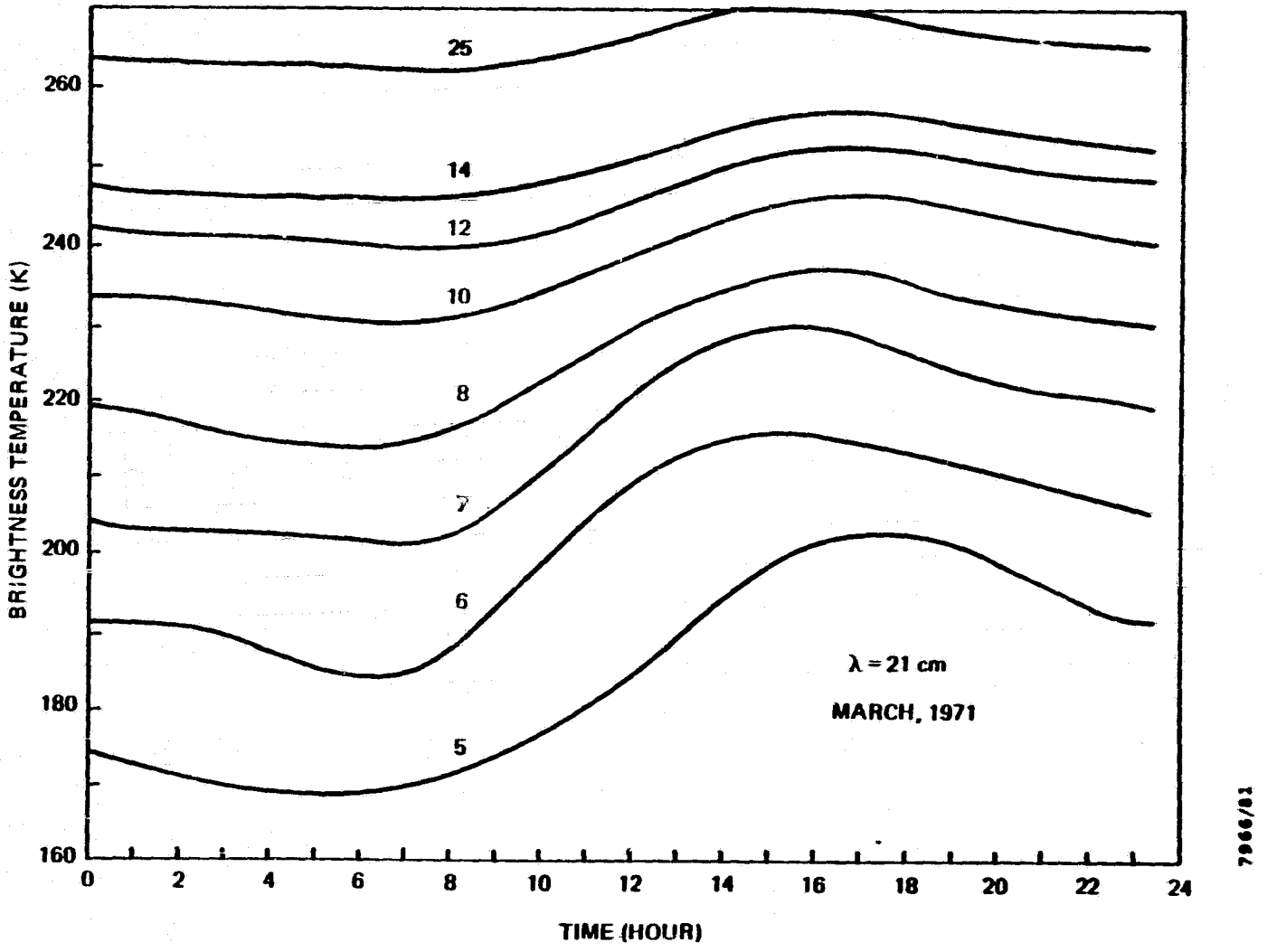

Figure 4. Typical diurnal variation of the calculated brightness temperature at λ = 21 cm (L-band) with the Arizona data. The days of March 1971 are marked on the curves.

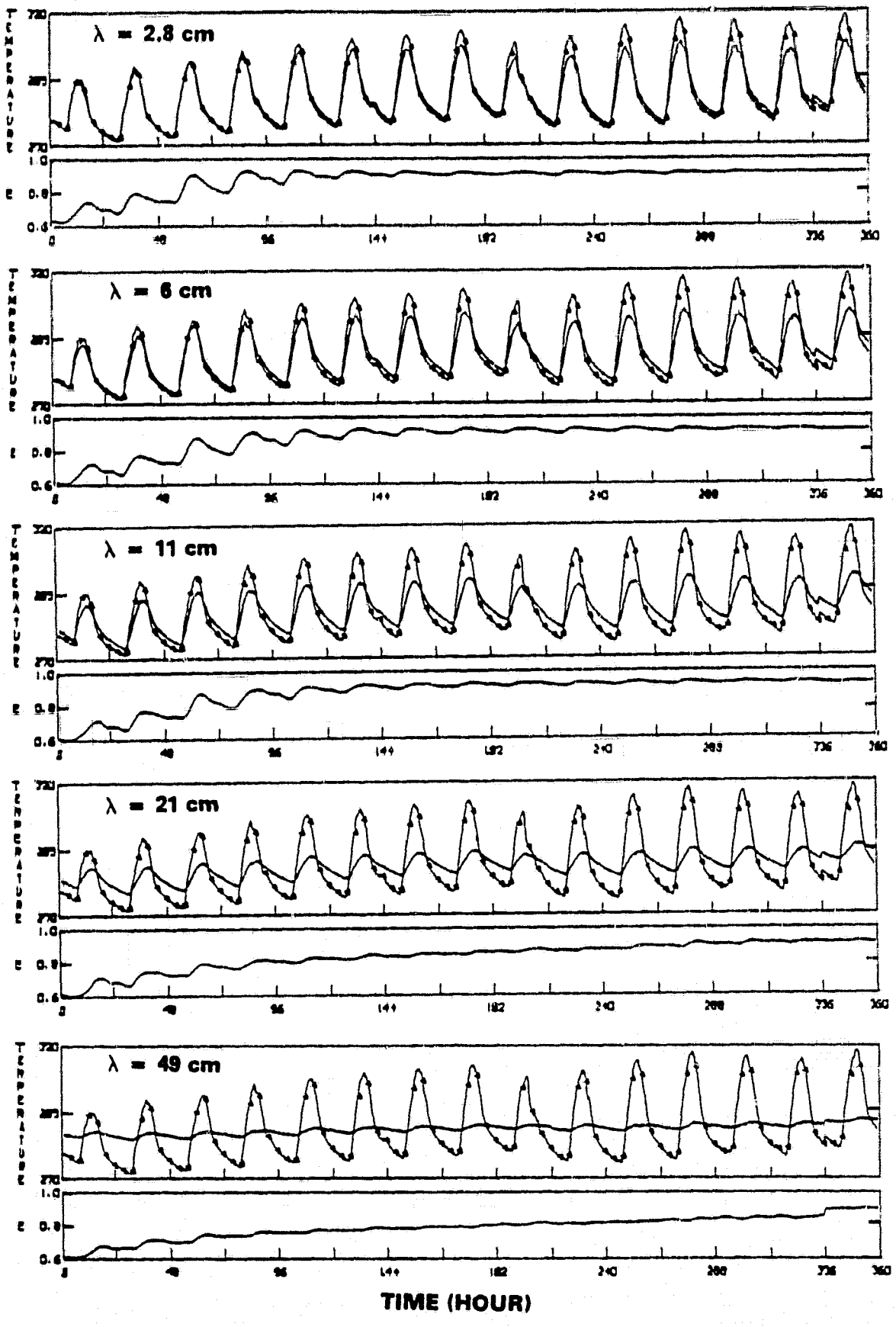

Figure 5. Synoptic view of the Arizona data (March 5-18 and 25, 1971): (1) Surface temperature (asterisk curves), (2) Effective temperature (solid curves on the upper parts), and (3) Emissivity (lower parts labeled by E). The small jumps at the 336th hour are due to 7-day gap in the data.

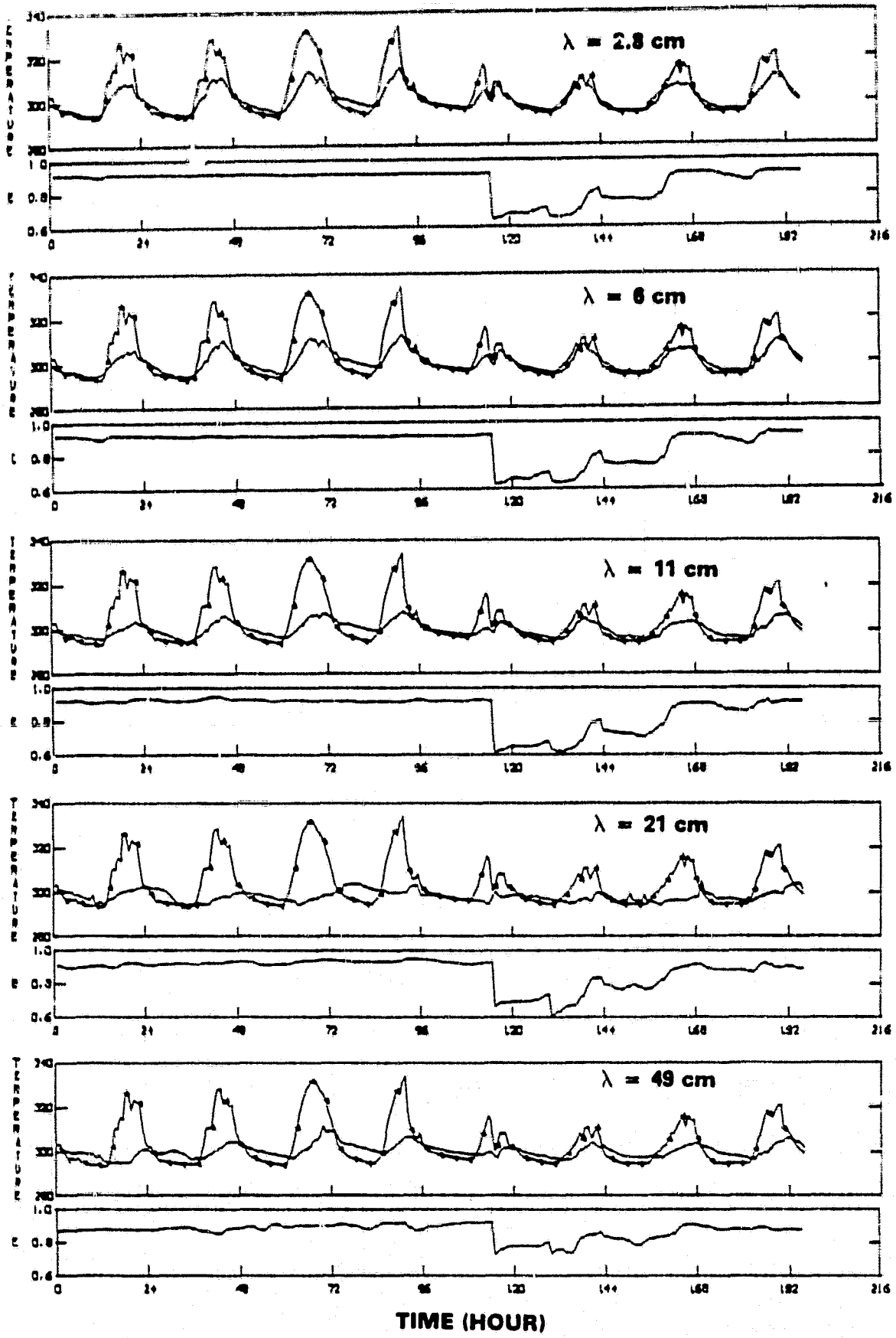

Figure 6. Synoptic view of the Georgia data (June 15-23, 1973): (1) Surface temperature (asterisk curves), (2) Effective temperature (solid curves on the upper parts), and (3) Emissivity (lower parts labeled by E). The 0th hour corresponds to 7 p.m., June 15, 1973. The sudden drops in emissivity between 110th and 140th hour are due to two rainfalls.

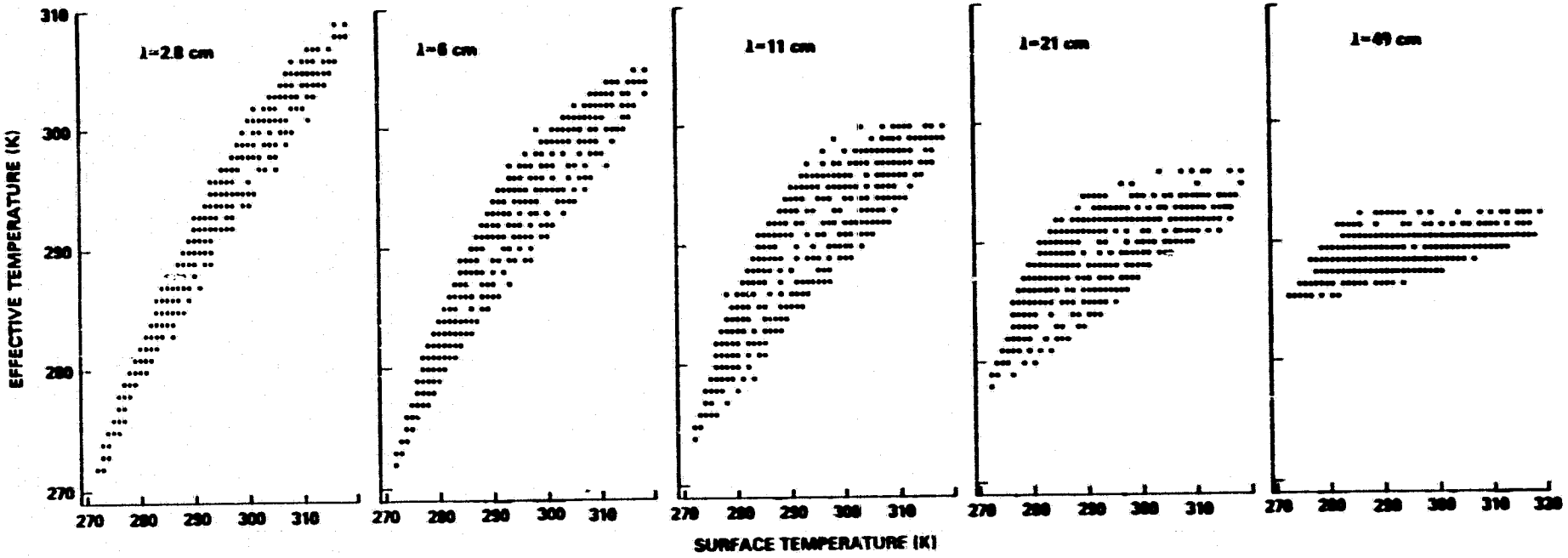

Figure 7. Calculated effective temperatures at five wavelengths (as marked) versus surface temperatures of Arizona data.

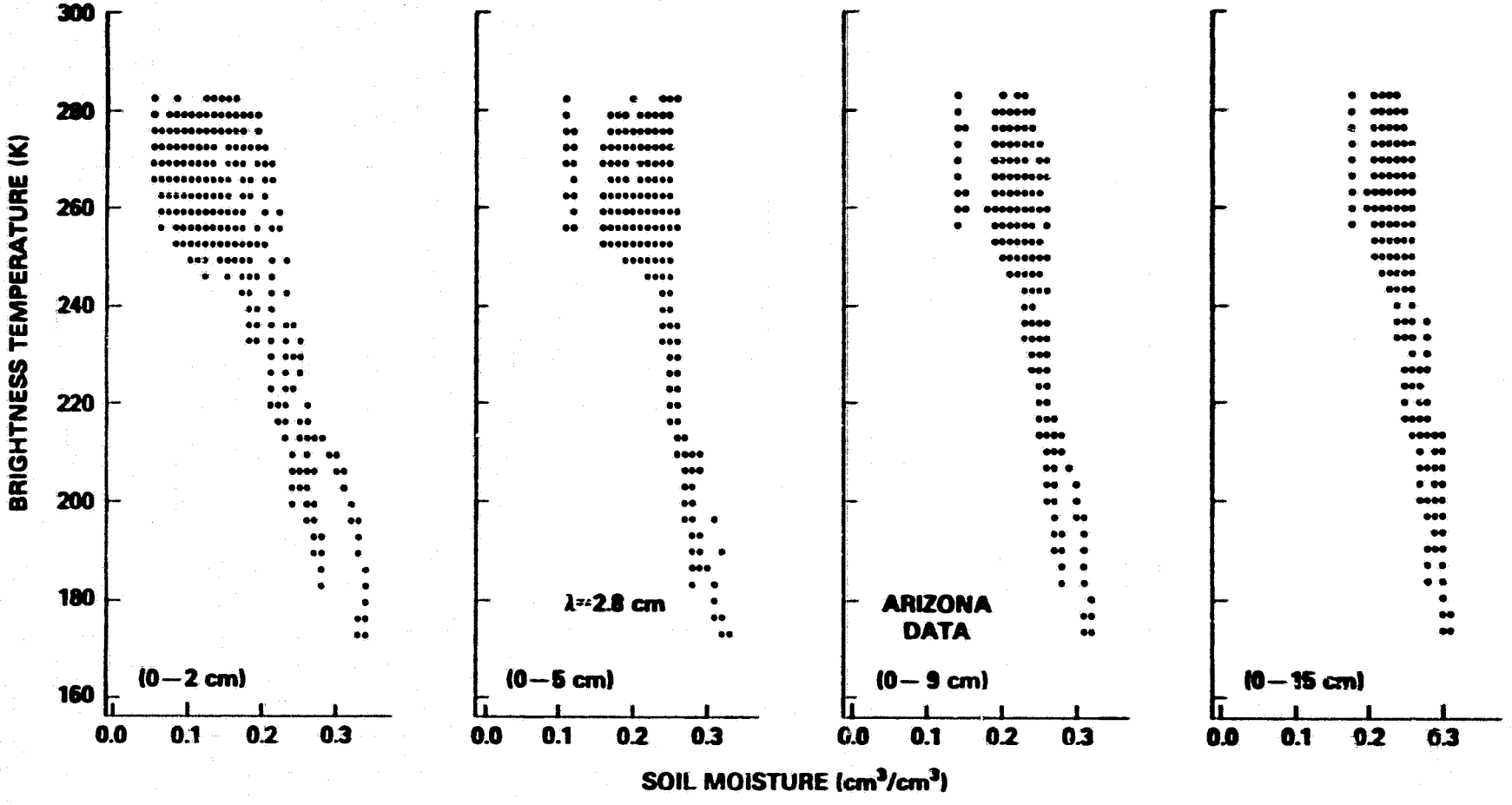

Figure 8(a). Brightness temperatures calculated with the Arizona data at λ = 2.8 cm and displayed as a function of soil moistures within the four soil depth intervals as labeled in the parentheses.

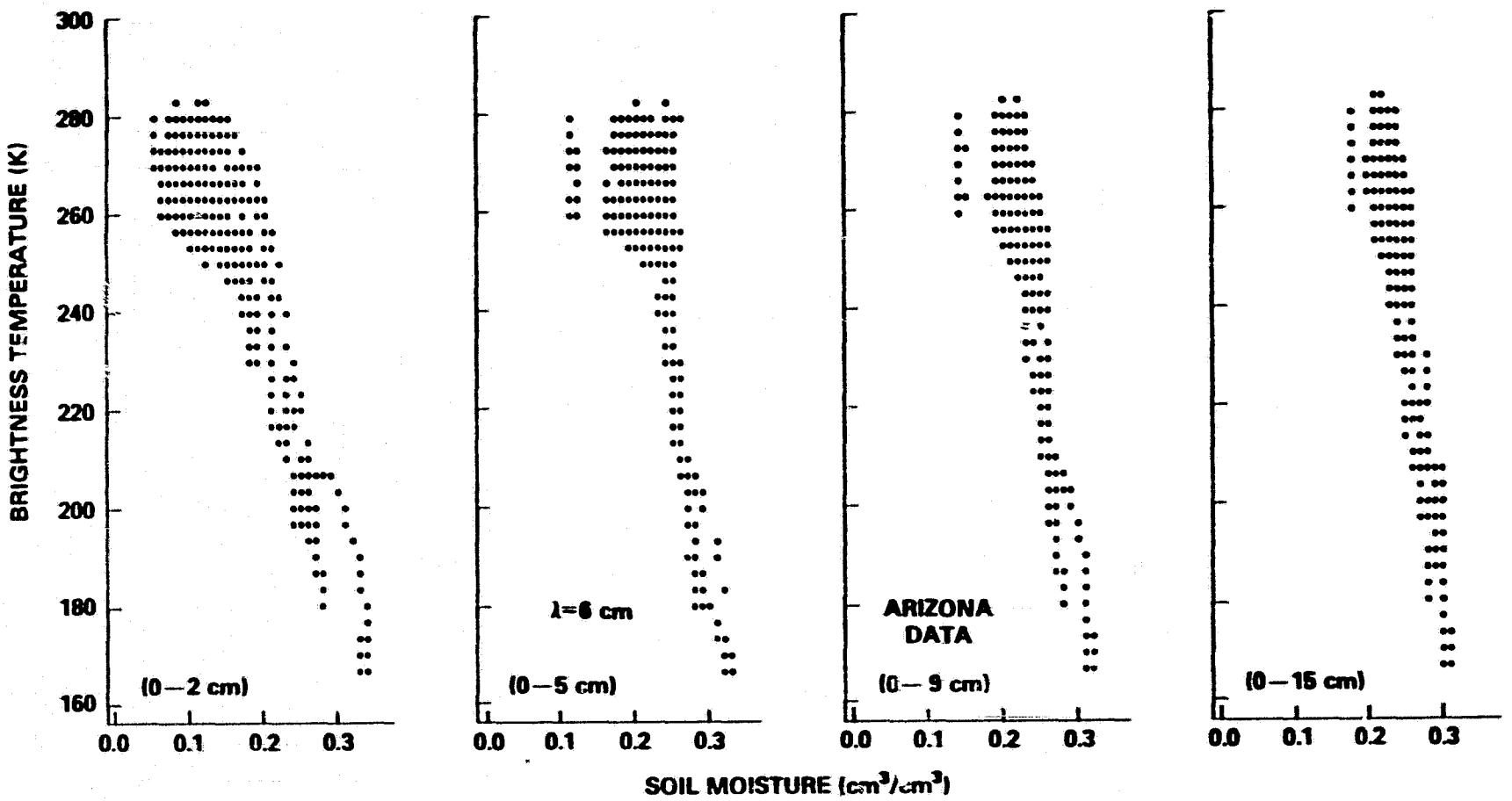

Figure 8(b). Brightness temperatures calculated with the Arizona data at λ = 6 cm and displayed as a function of soil moistures within the four soil depth intervals as labeled in the parentheses.

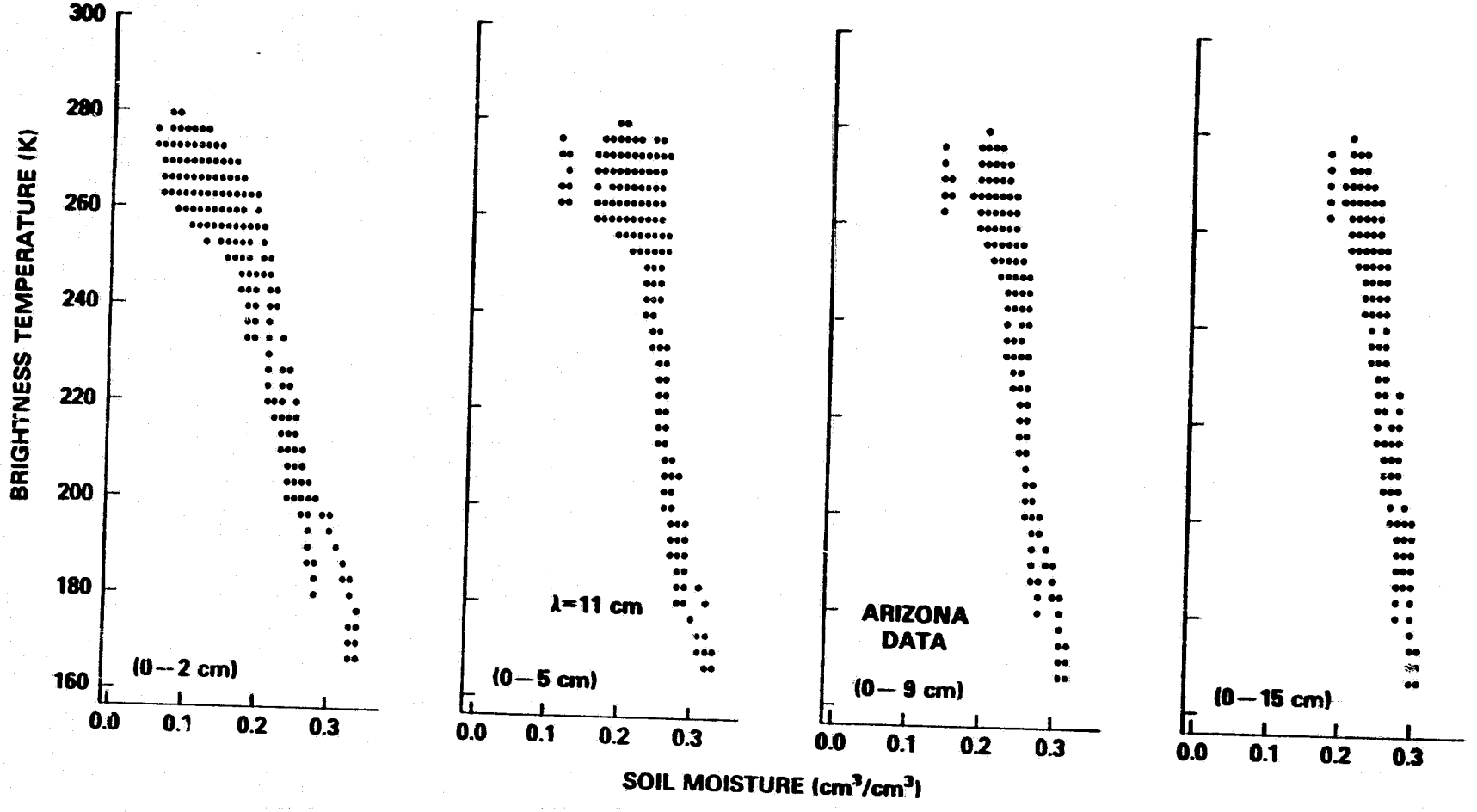

Figure 8(c). Brightness temperatures calculated with the Arizona data at λ = 11 cm and displayed as a function of soil moistures within the four soil depth intervals as labeled in the parentheses.

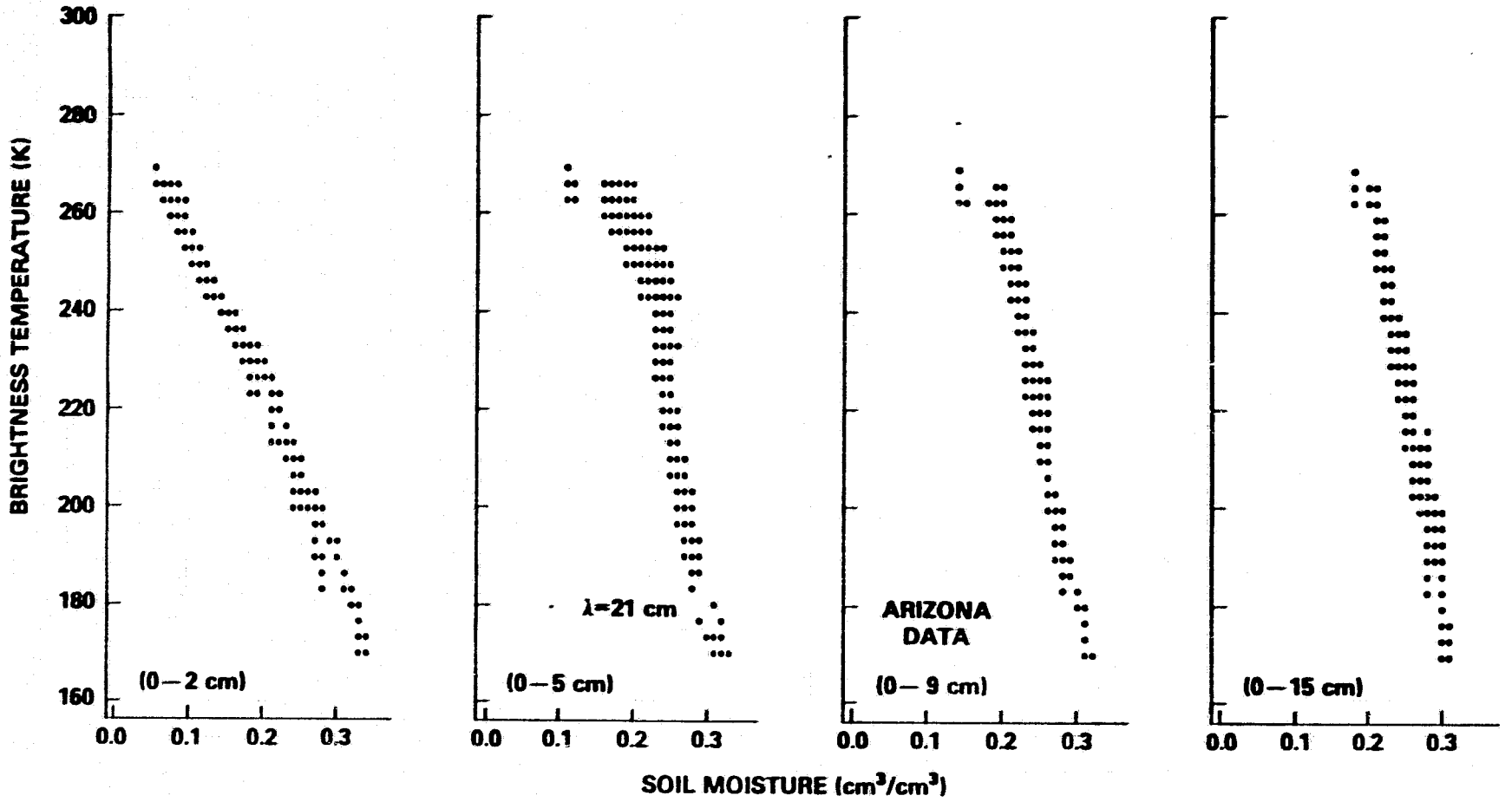

Figure 8(d). Brightness temperatures calculated with the Arizona data at λ = 21 cm and displayed as a function of soil moistures within the four soil depth intervals as labeled in the parentheses.

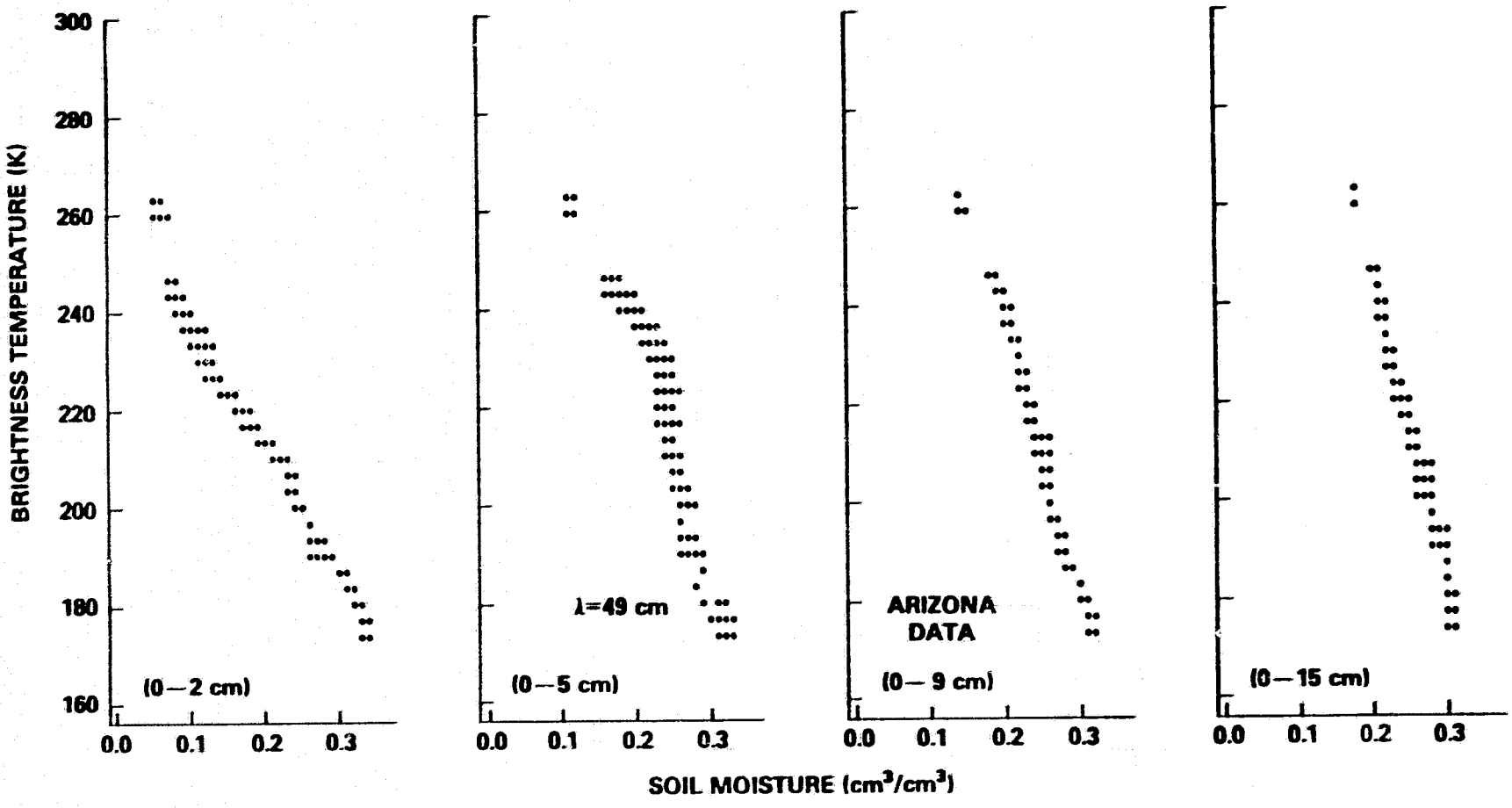

Figure 8(e). Brightness temperatures calculated with the Arizona data at λ = 49 cm and displayed as a function of soil moistures within the four soil depth intervals as labeled in the parentheses.

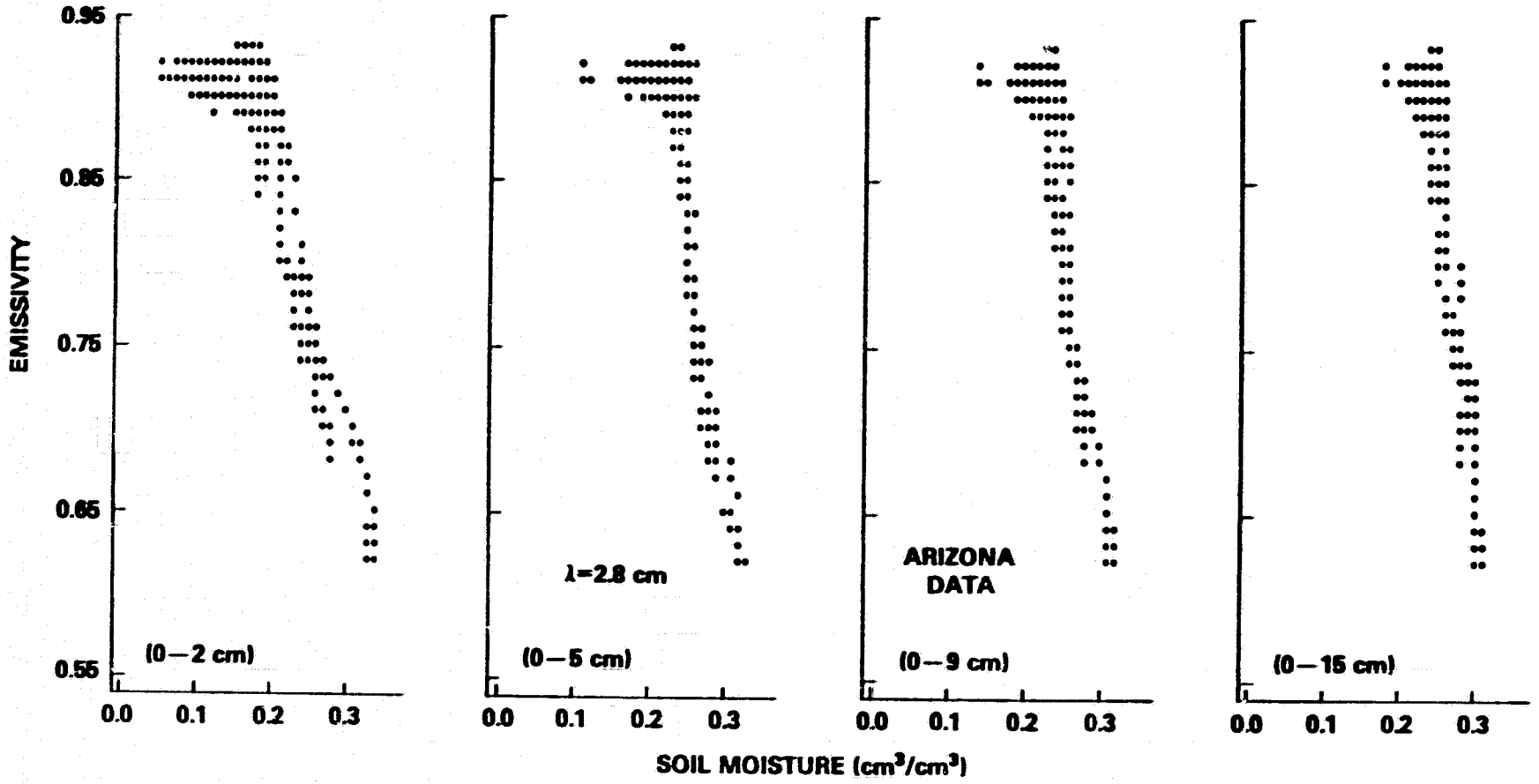

Figure 9(a). Emissivities calculated with the Arizona data at λ = 2.8 cm and displayed as a function of soil moistures within the four soil depth intervals as marked in the parentheses.

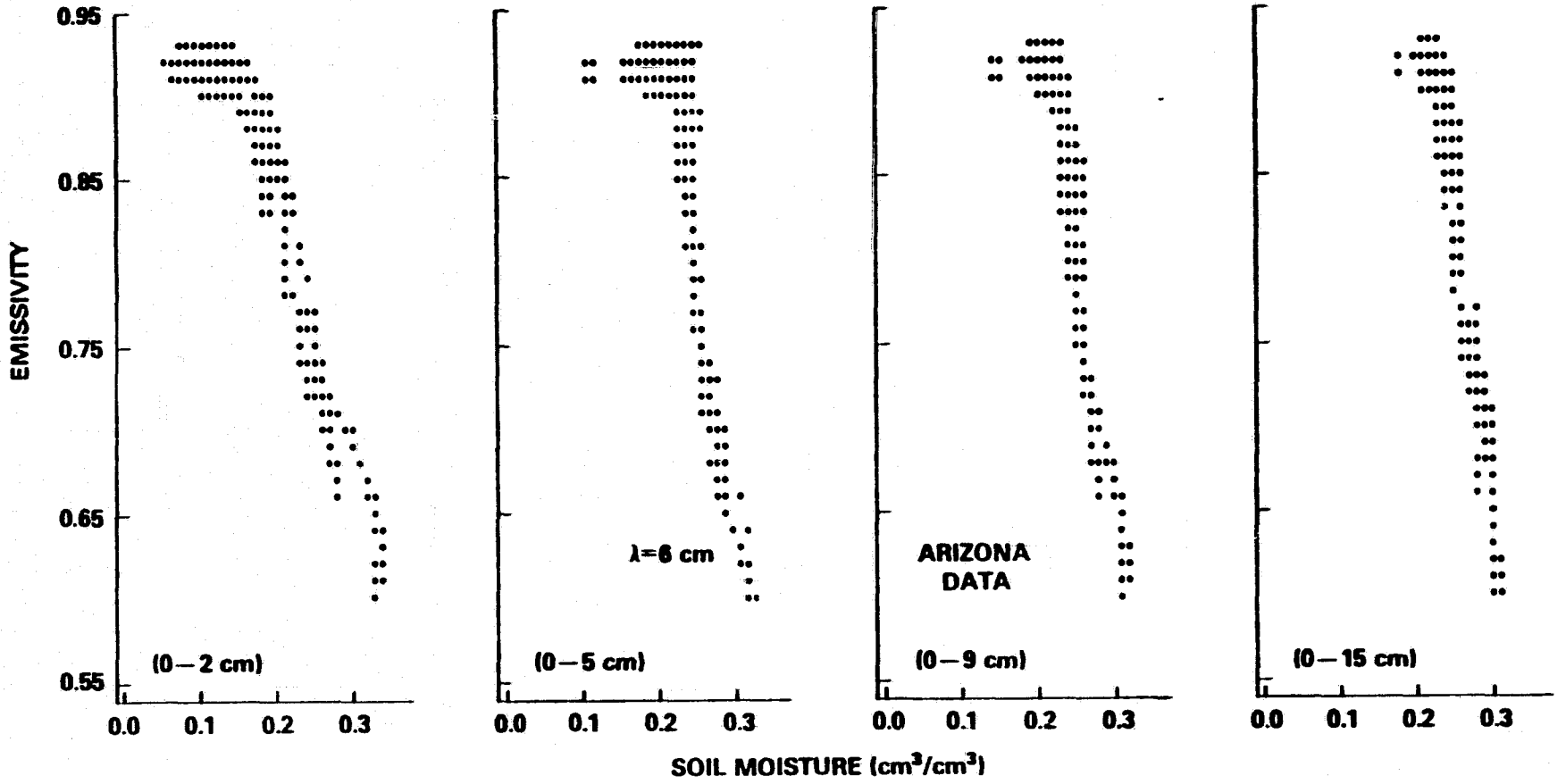

Figure 9(b). Emissivities calculated with the Arizona data at λ = 6 cm and displayed as a function of soil moistures within the four soil depth intervals as marked in the parentheses.

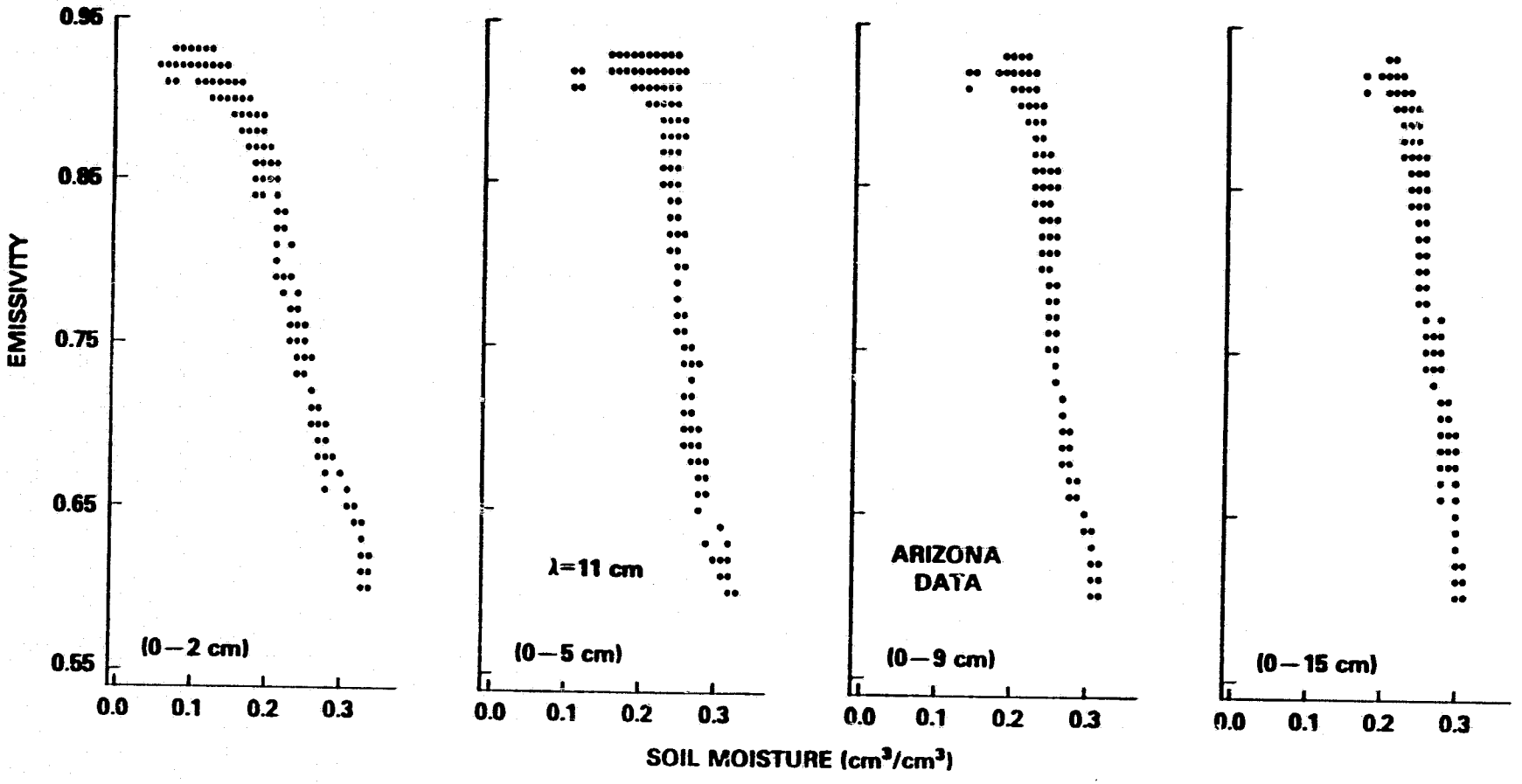

Figure 9(c). Emissivities calculated with the Arizona data at λ = 11 cm and displayed as a function of soil moistures within the four soil depth intervals as marked in the parentheses.

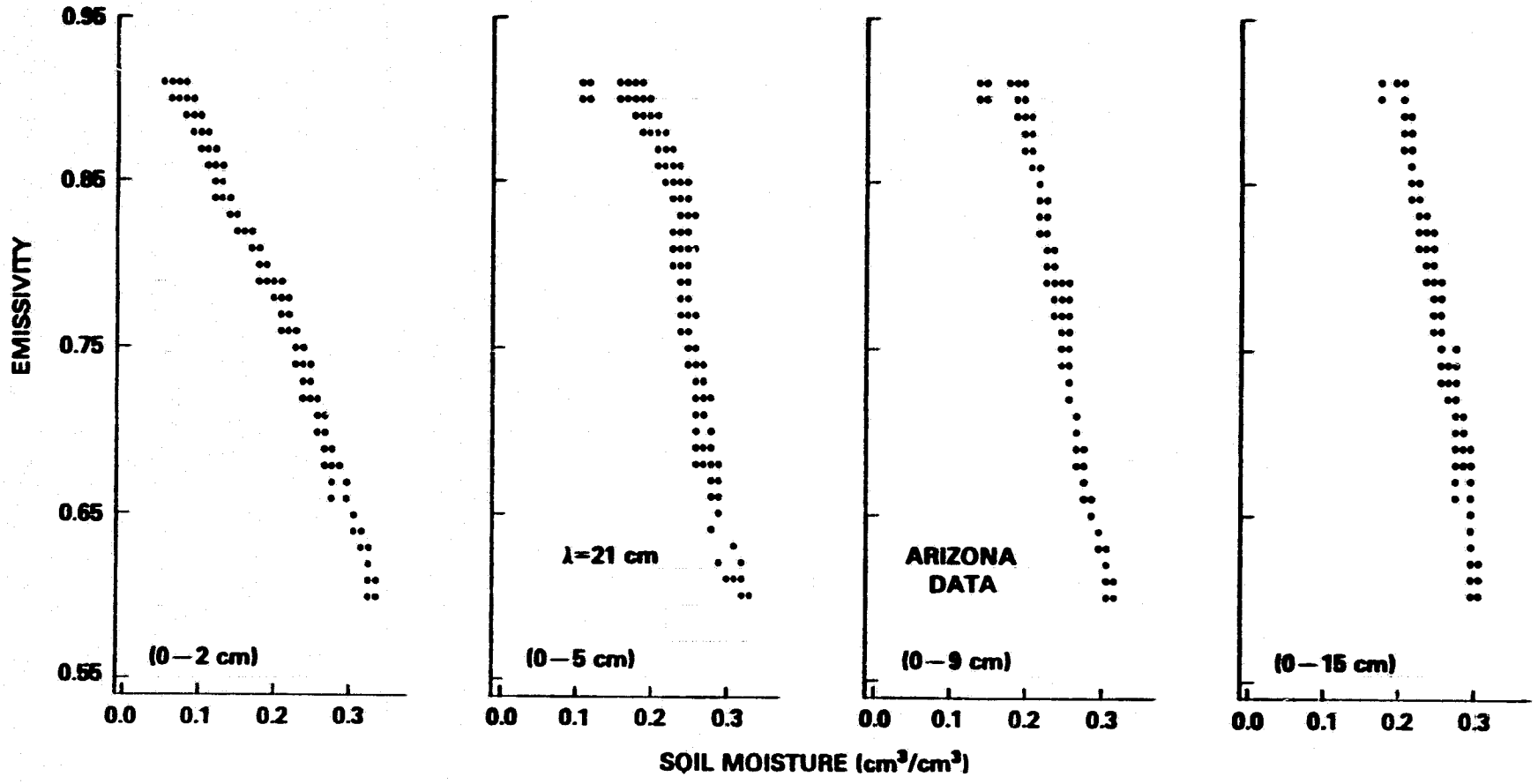

Figure 9(d). Emissivities calculated with the Arizona data at λ = 21 cm and displayed as a function of soil moistures within the four soil depth intervals as marked in the parentheses.

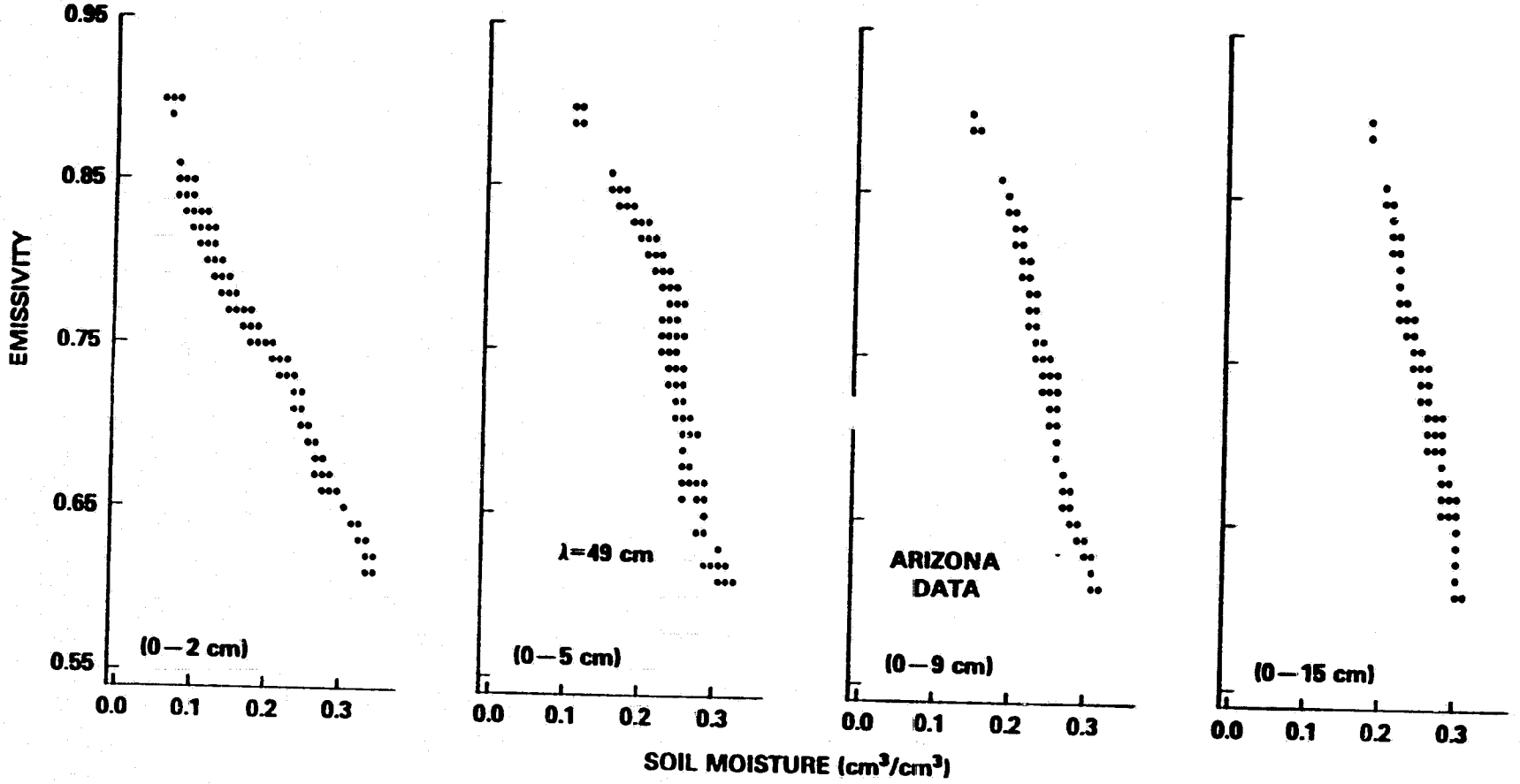

Figure 9(e). Emissivities calculated with the Arizona data at λ = 49 cm and displayed as a function of soil moistures within the four soil depth intervals as marked in the parentheses.

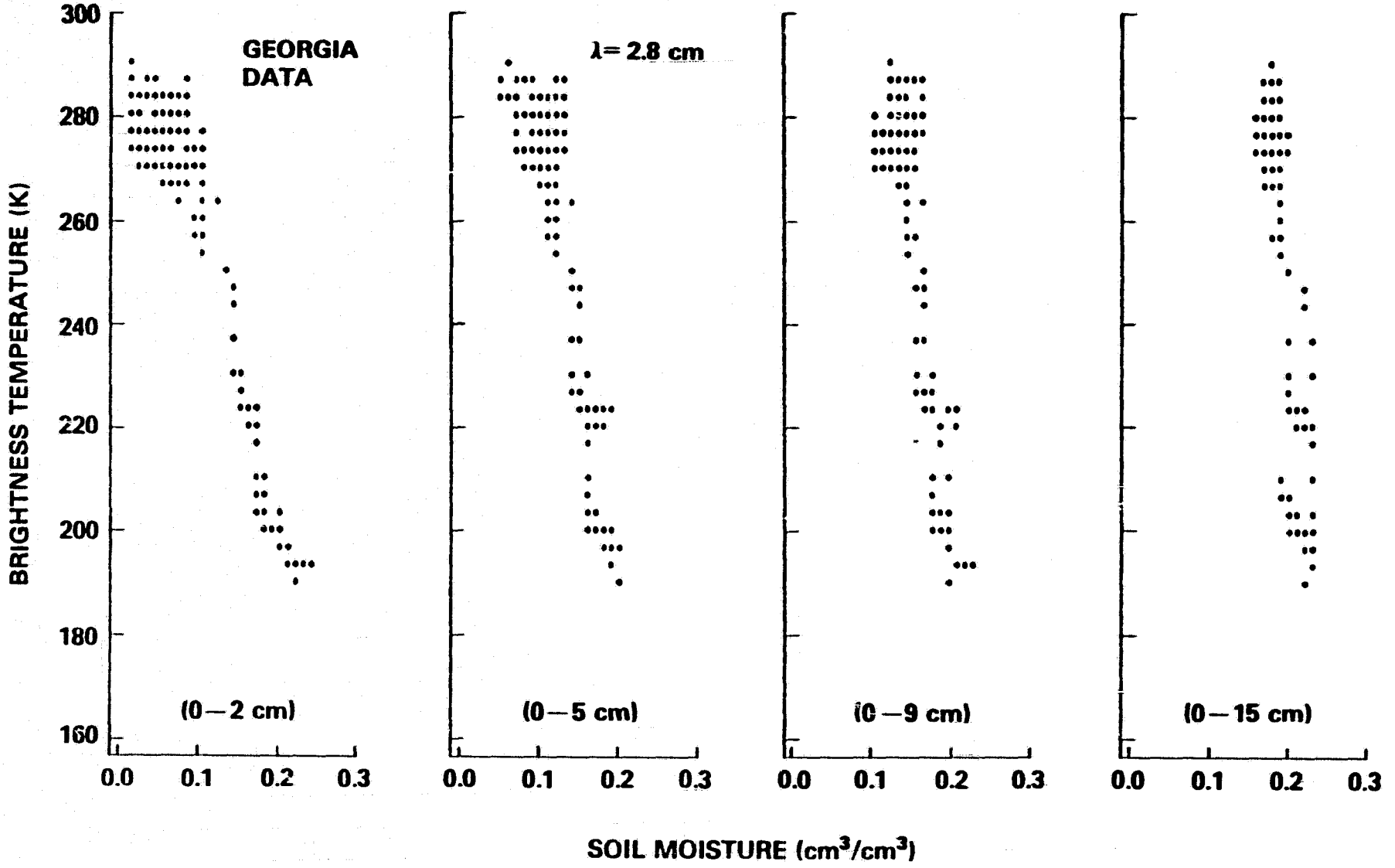

Figure 10(a). Brightness temperatures calculated with the Georgia data at λ = 2.8 cm and displayed as a function of soil moistures within the four soil depth intervals as labeled in the parentheses.

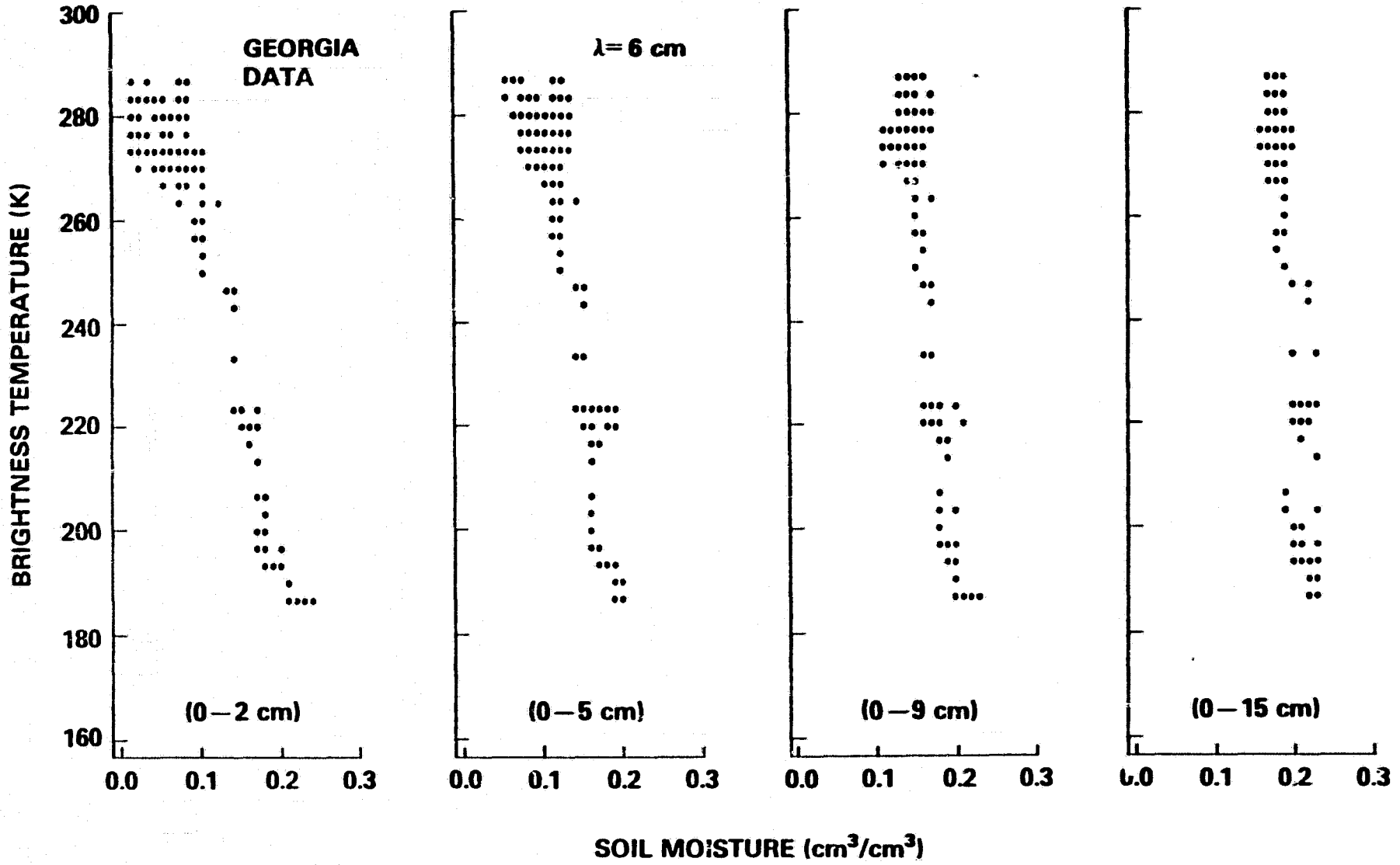

Figure 10(b). Brightness temperatures calculated with the Georgia data at λ = 6 cm and displayed as a function of soil moistures within the four soil depth intervals as labeled in the parentheses.

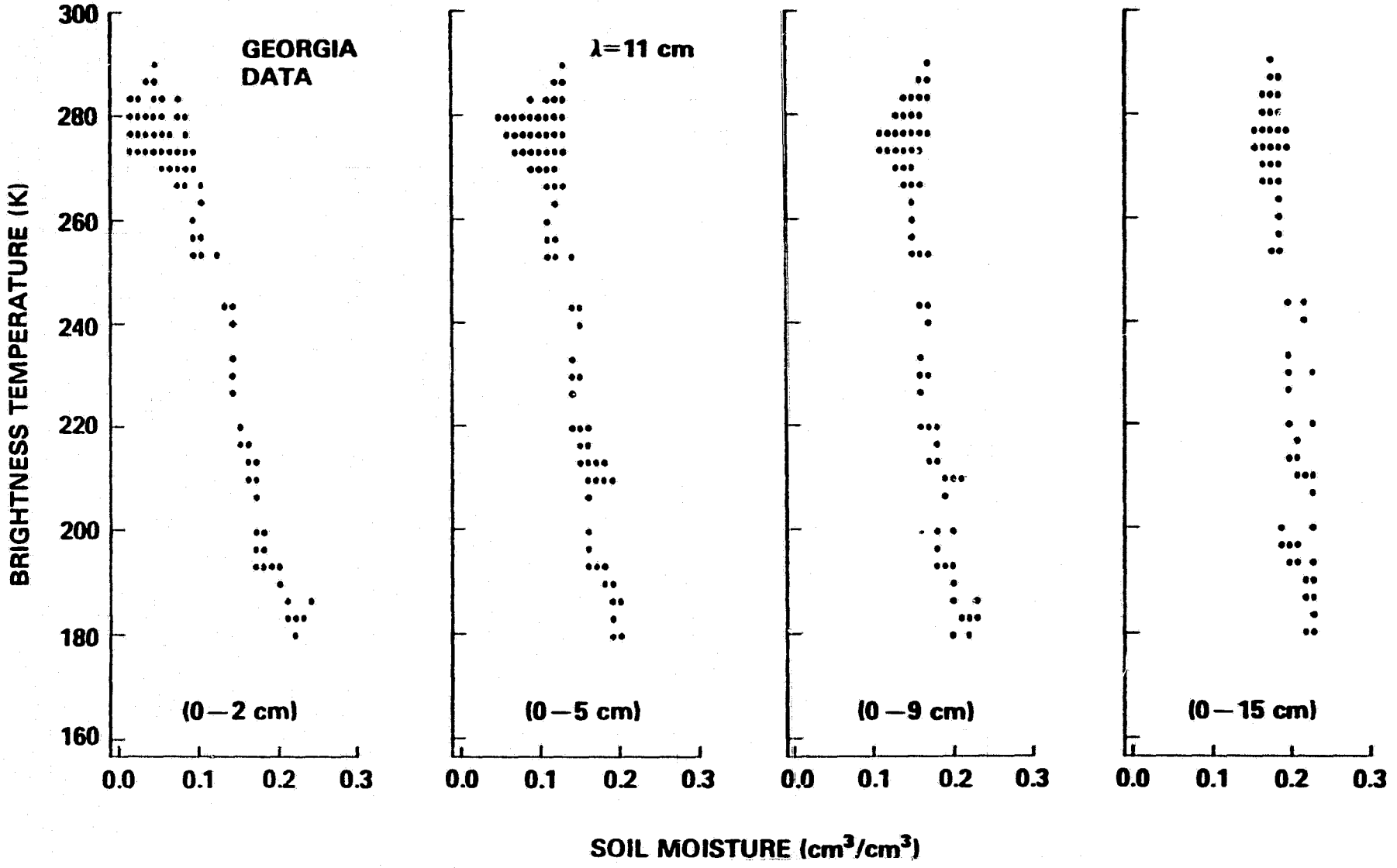

Figure 10(c). Brightness temperatures calculated with the Georgia data at λ = 11 cm and displayed as a function of soil moistures within the four soil depth intervals as labeled in the parentheses.

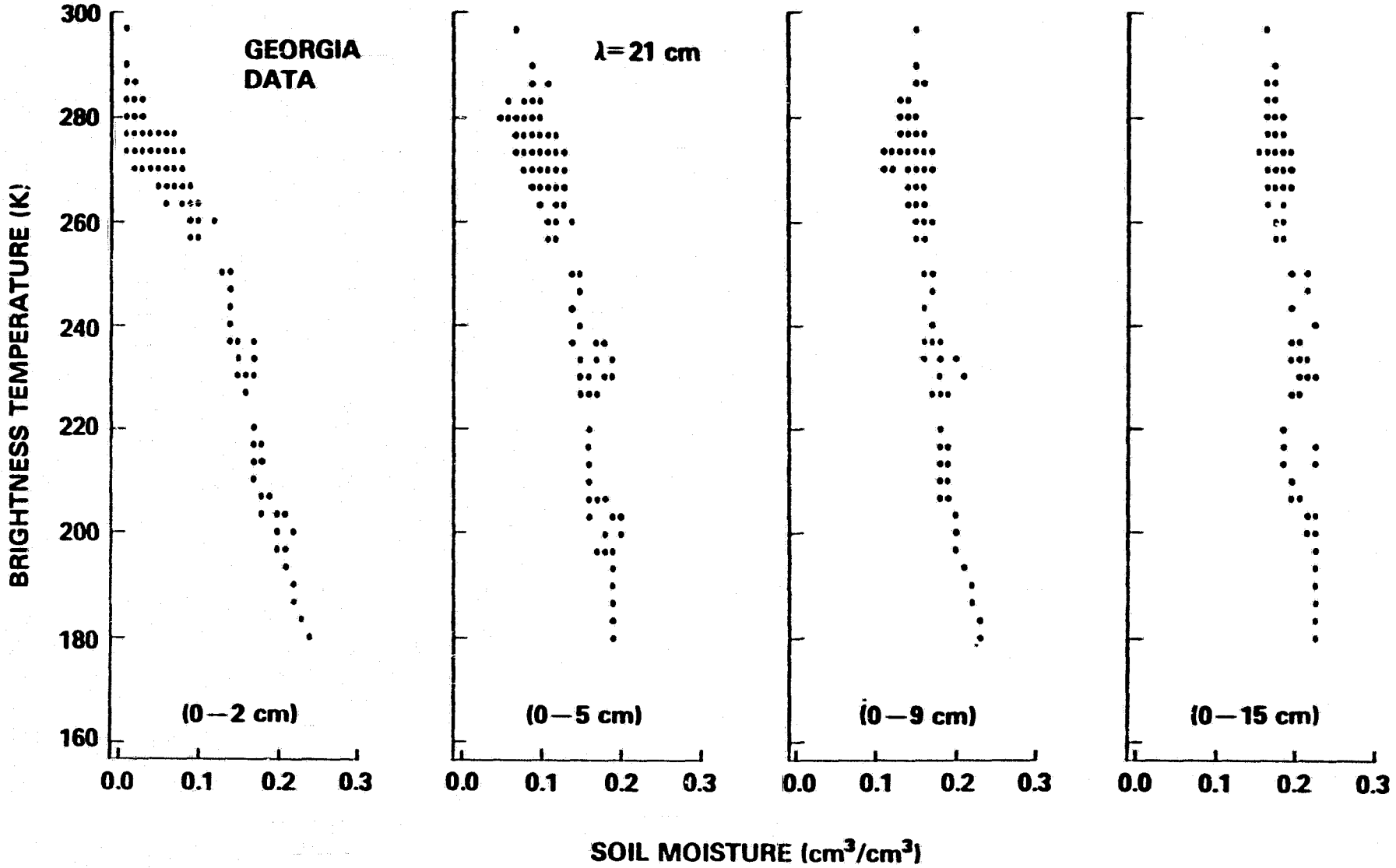

Figure 10(d). Brightness temperatures calculated with the Georgia data at λ = 21 cm and displayed as a function of soil moistures within the four soil depth intervals as labeled in the parentheses.

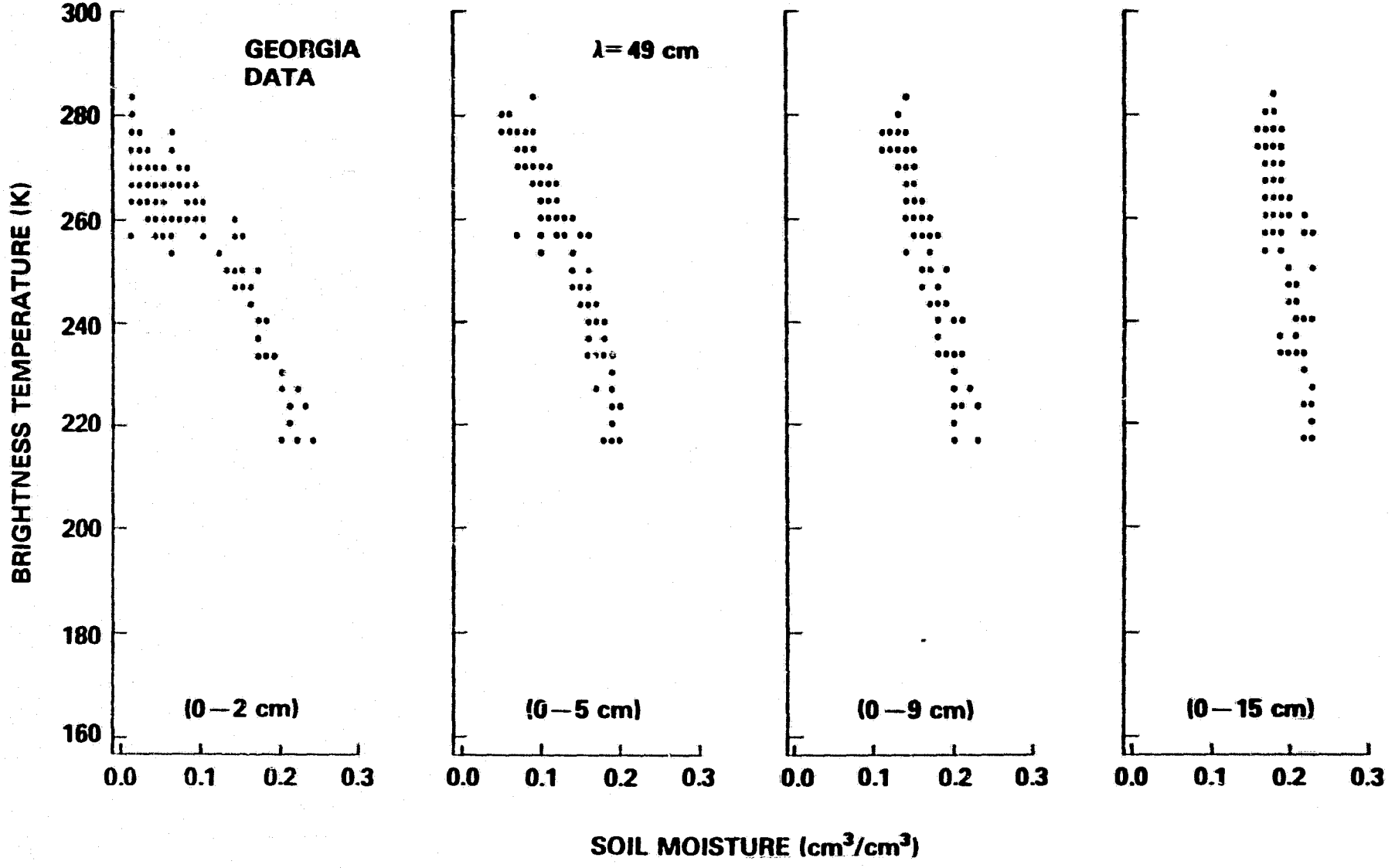

Figure 10(e). Brightness temperatures calculated with the Georgia data at λ = 49 cm and displayed as a function of soil moistures within the four soil depth intervals as labeled in the parentheses.

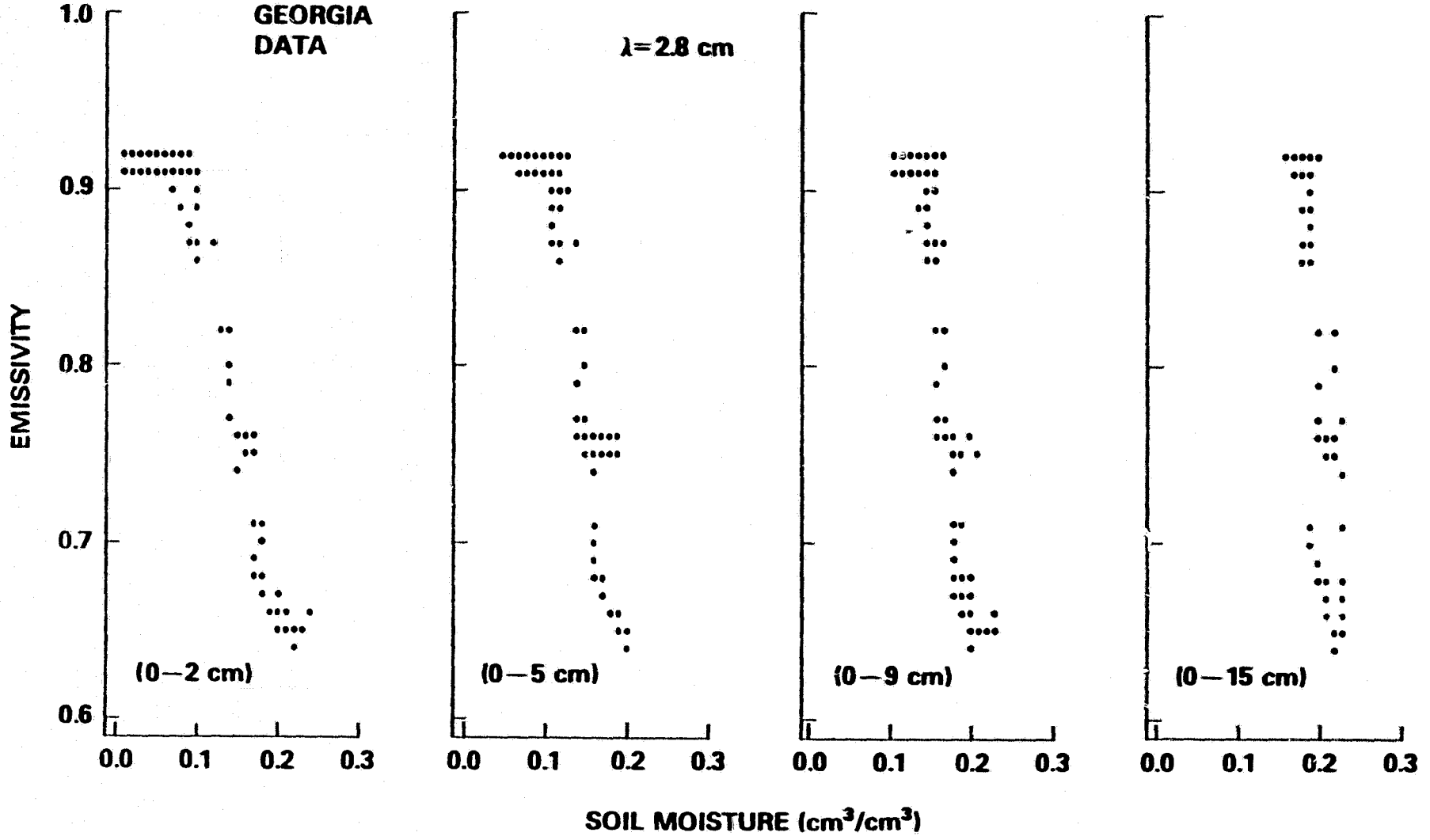

Figure 11(a). Emissivities calculated with the Georgia data at λ = 2.8 cm and displayed as a function of soil moistures within the four soil depth intervals as marked in the parentheses.

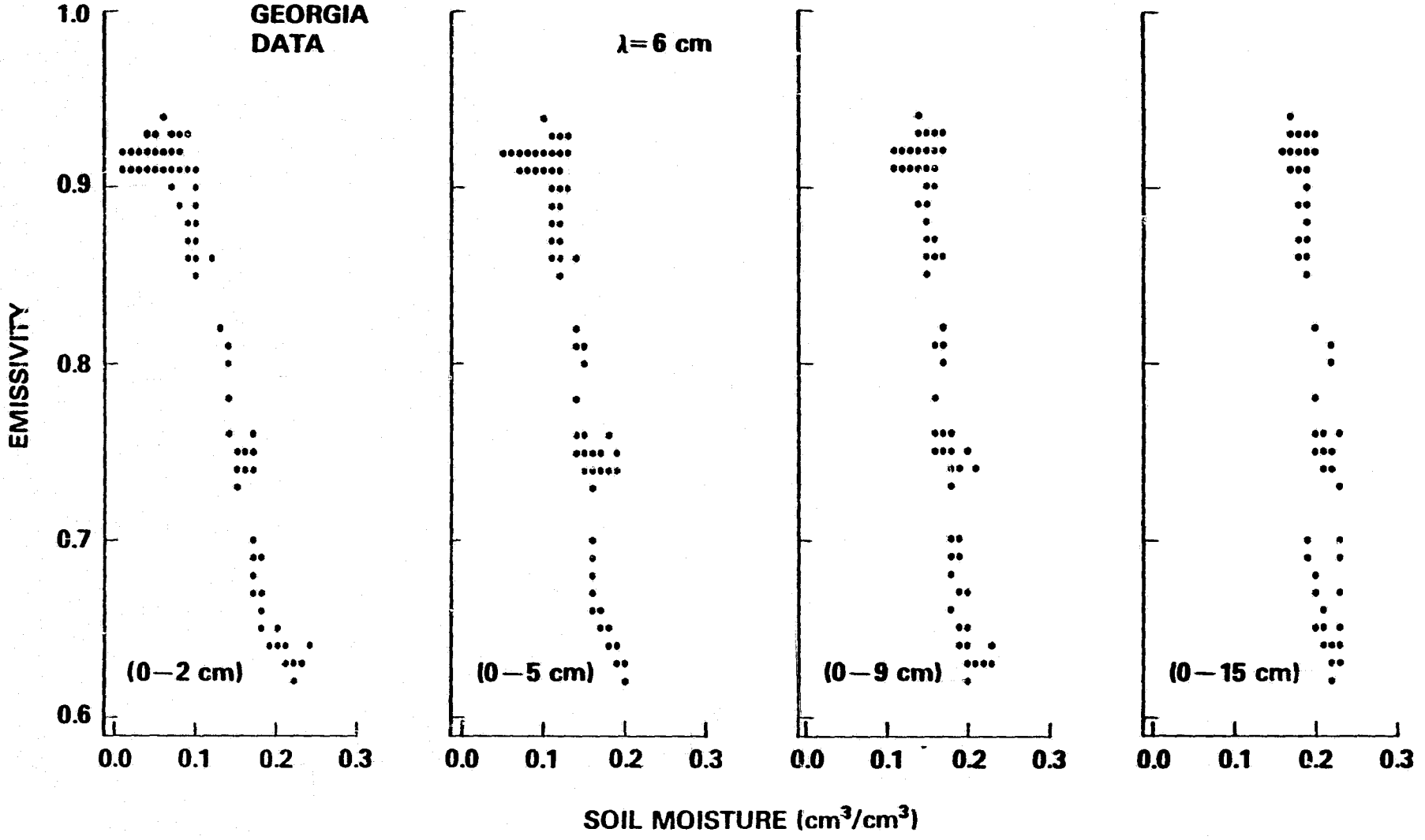

Figure 11(b). Emissivities calculated with the Georgia data at λ = 6 cm and displayed as a function of soil moistures within the four soil depth intervals as marked in the parentheses.

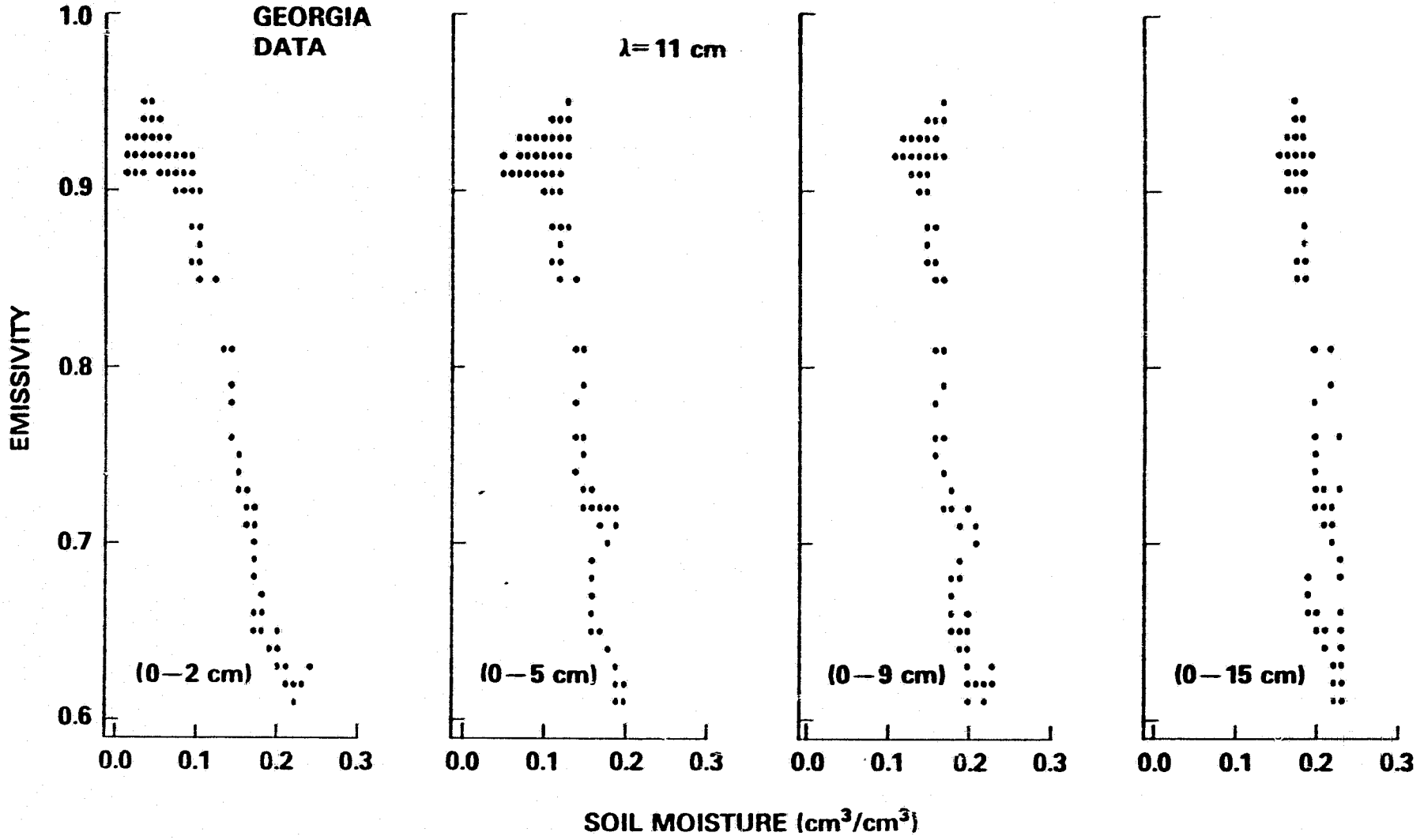

Figure 11(c). Emissivities calculated with the Georgia data at λ = 11 cm and displayed as a function of soil moistures within the four soil depth intervals as marked in the parentheses.

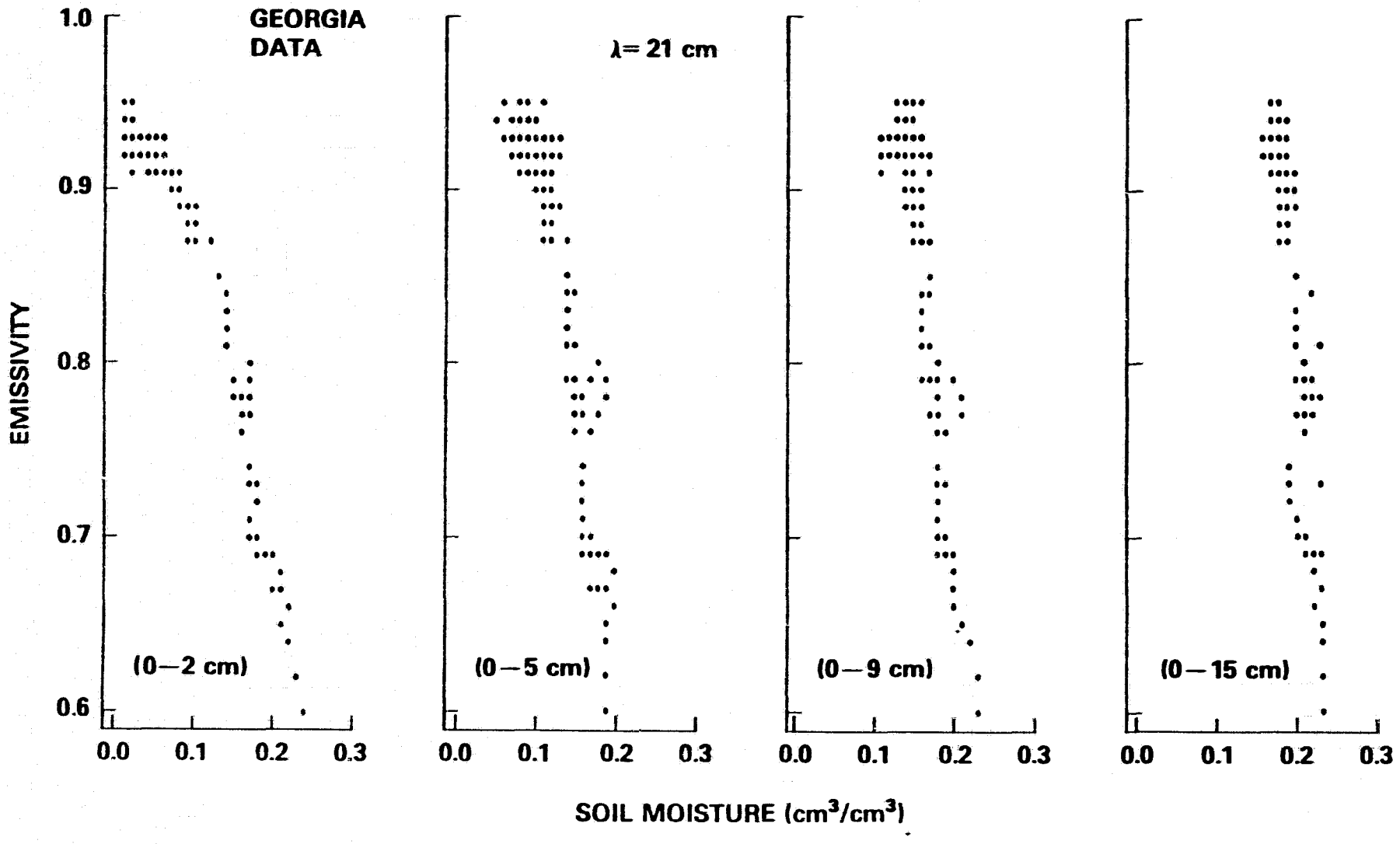

Figure 11(d). Emissivities calculated with the Georgia data at λ = 21 cm and displayed as a function of soil moistures within the four soil depth intervals as marked in the parentheses.

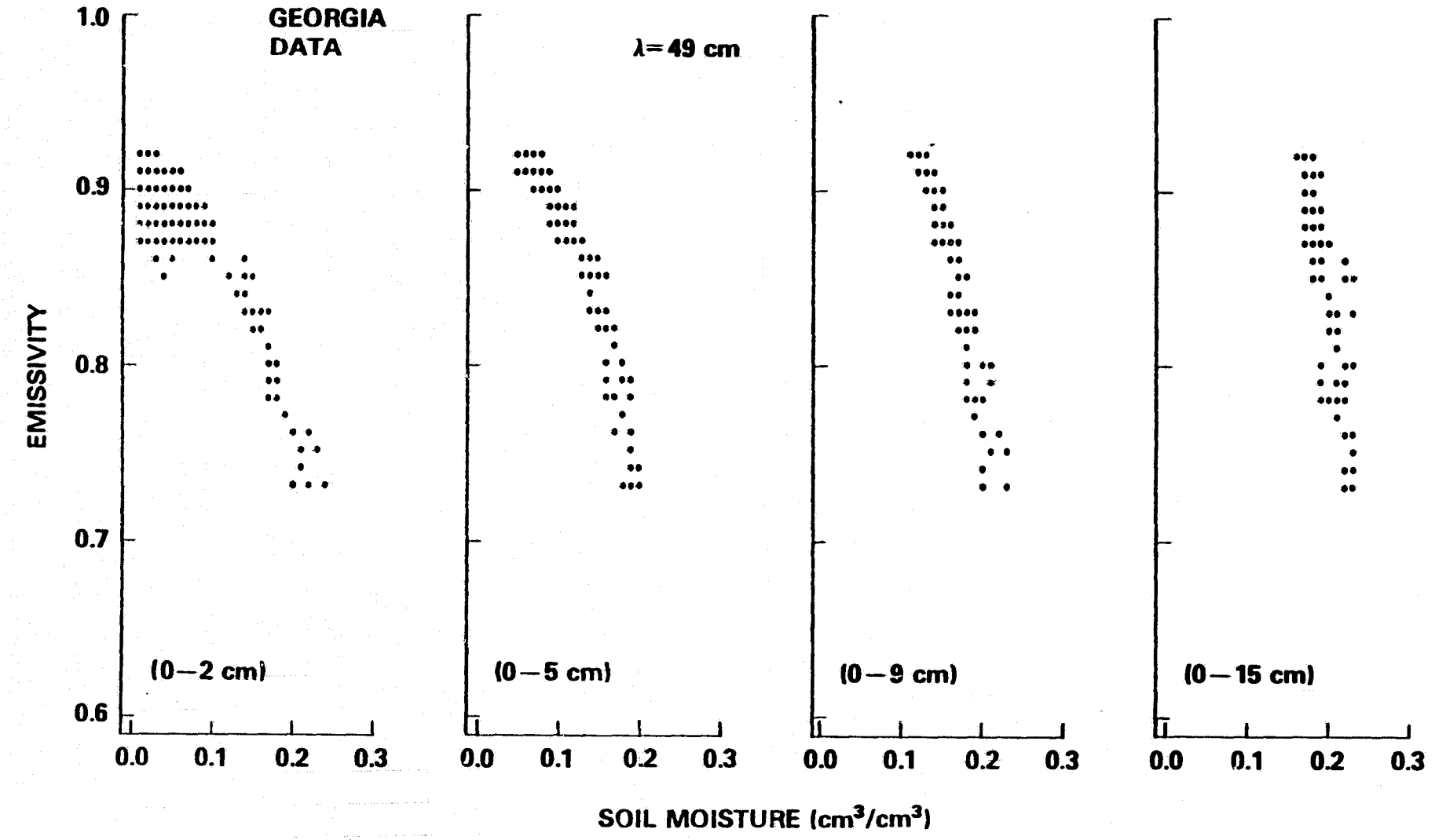

Figure 11(e). Emissivities calculated with the Georgia data at λ = 49 cm and displayed as a function of soil moistures within the four soil depth intervals as marked in the parentheses.

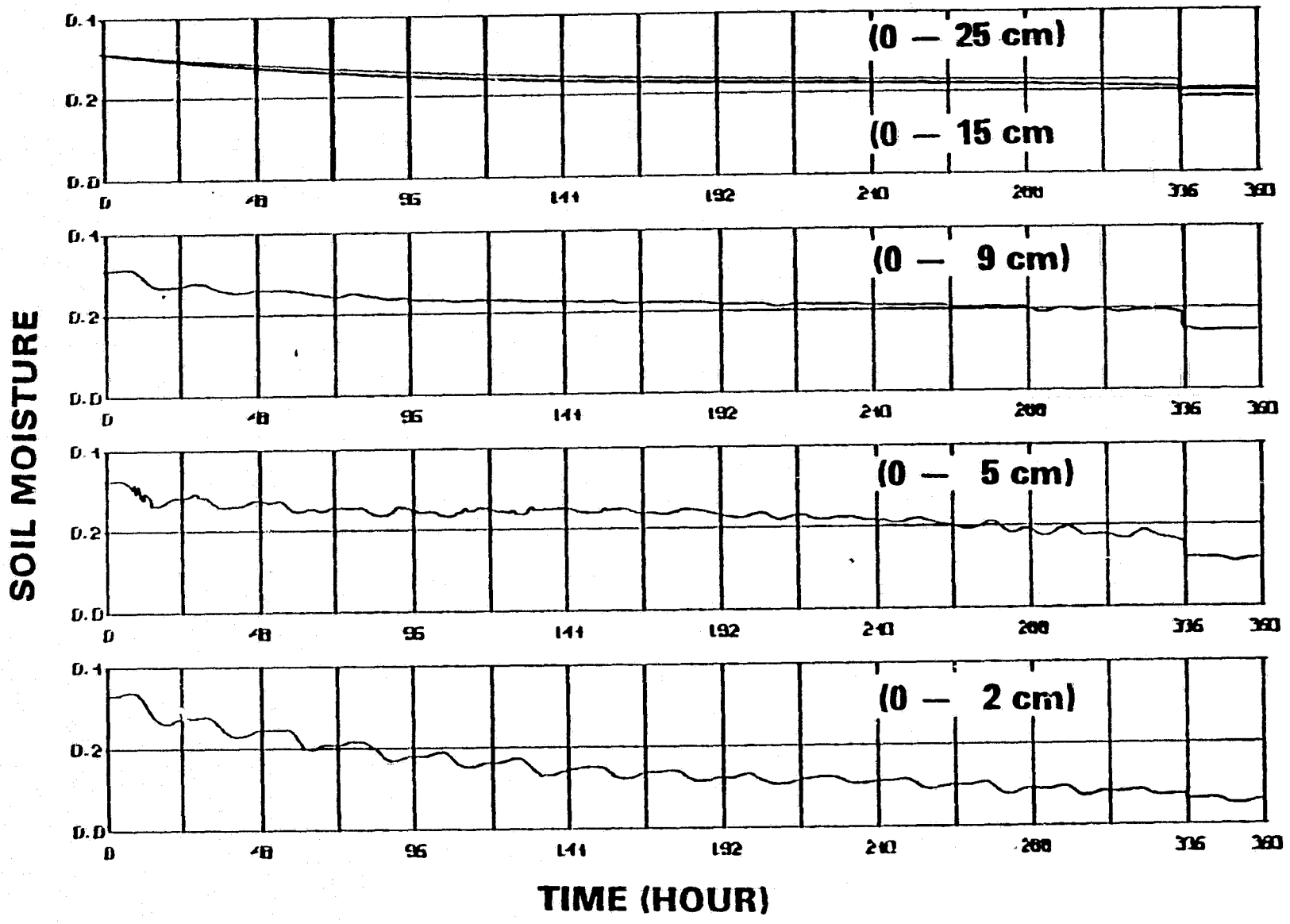

Figure 12. Soil moistures (from Arizona data) within the depth intervals of 0-2, 0-5, 0-9, 0-15, and 0-25 cm. The first four groups are employed in the present work for the statistical analysis of the calculated brightness temperature and emissivity, as shown in Figures 8-11. The 0-25 cm layer is shown here for comparison with that of 0-15 cm layer. The sudden drops at the 336th hour are due to 7-day gap in the data.

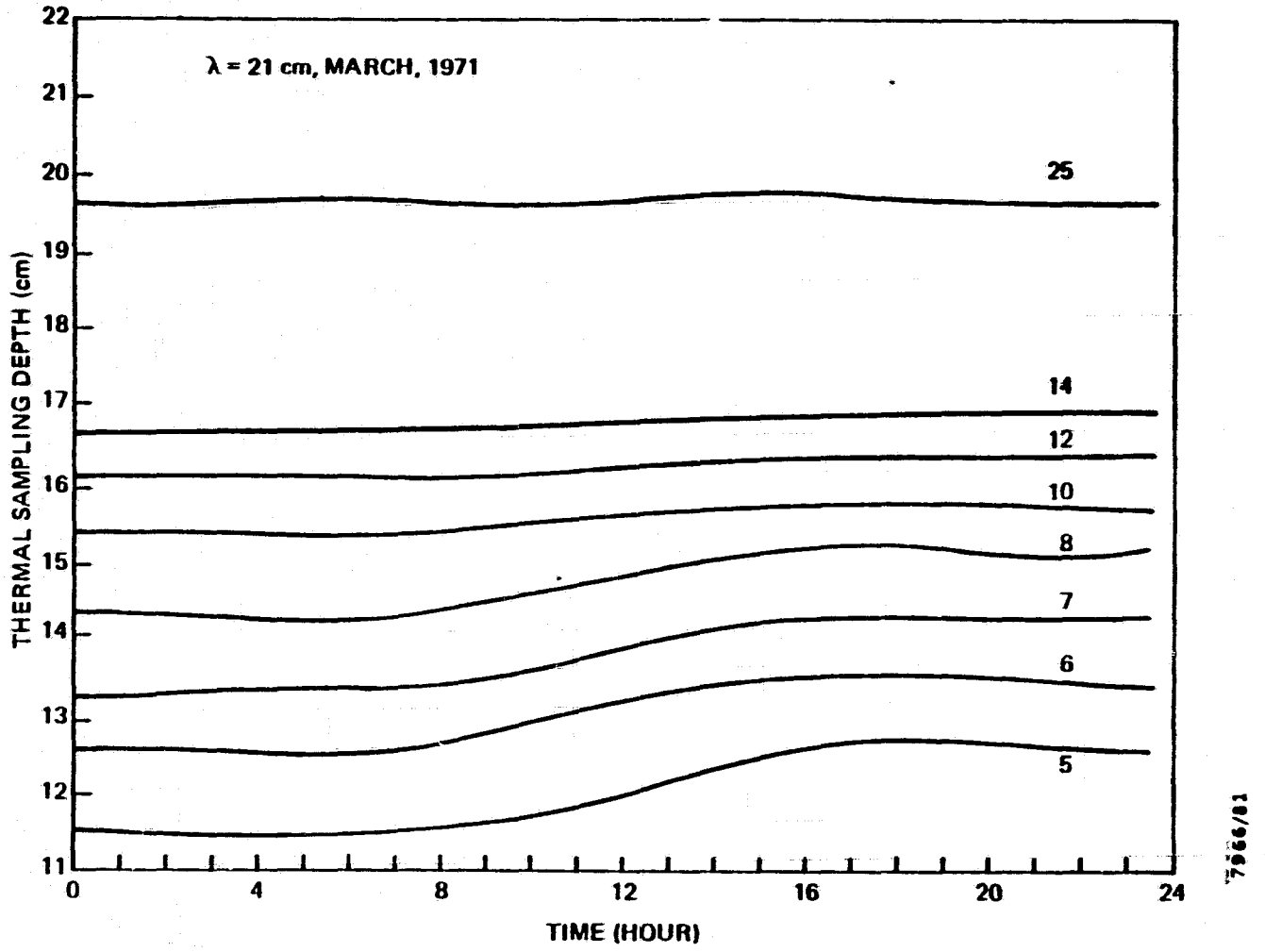

Figure 13. Diurnal variation of the thermal sampling depths calculated with the Arizona data at λ = 21 cm. It should be noted that the values for March 25 (dry soil condition) are approximately equal to 0.96λ. The dates of March 1971 are marked on the curves.

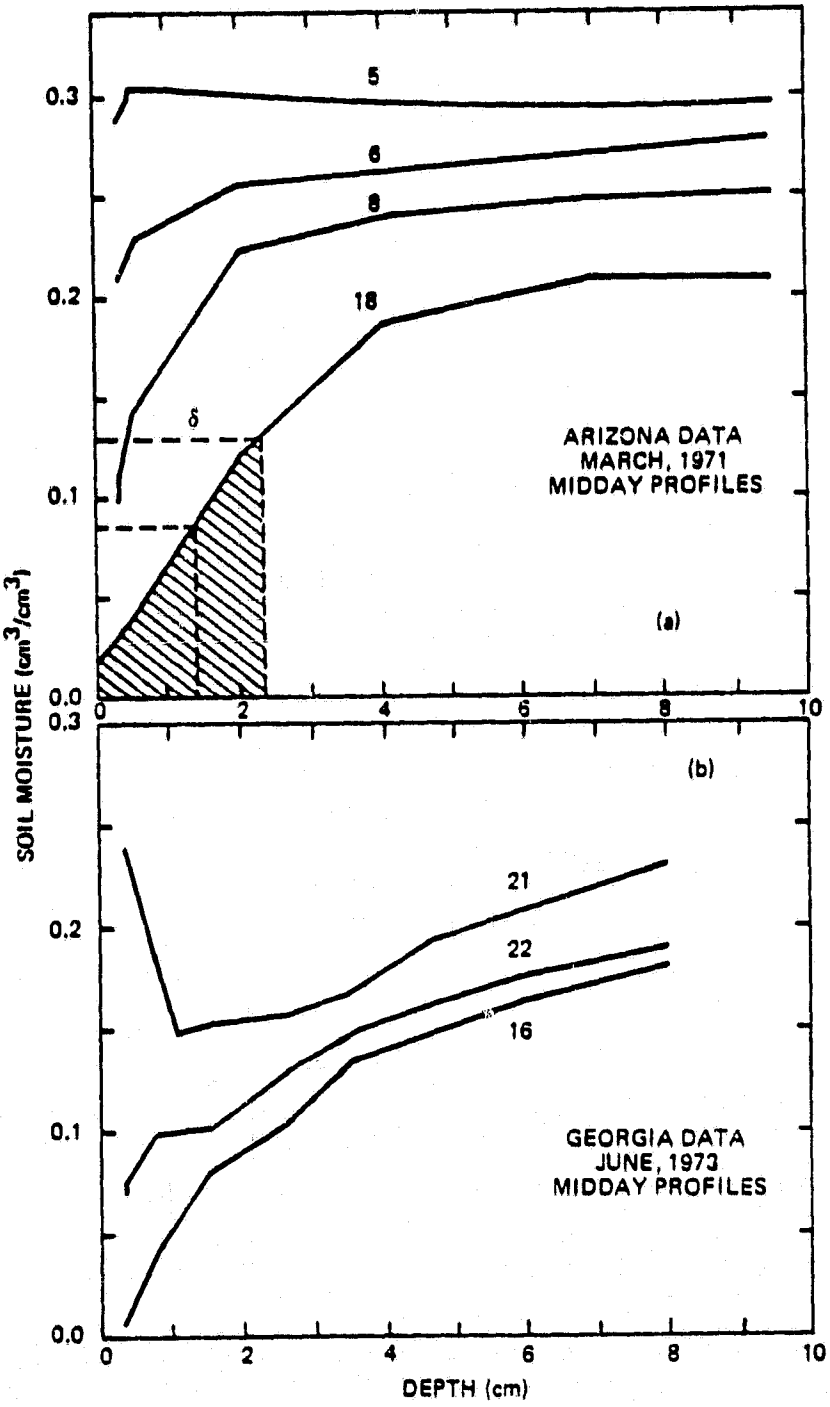

Figure 14. Selected moisture profiles (at midday). The dates of observation of these profiles are labeled on the curves, (a) Arizona data and (b) Georgia data. The shaded area is used to determine the moisture sampling depth δ as described in the text.

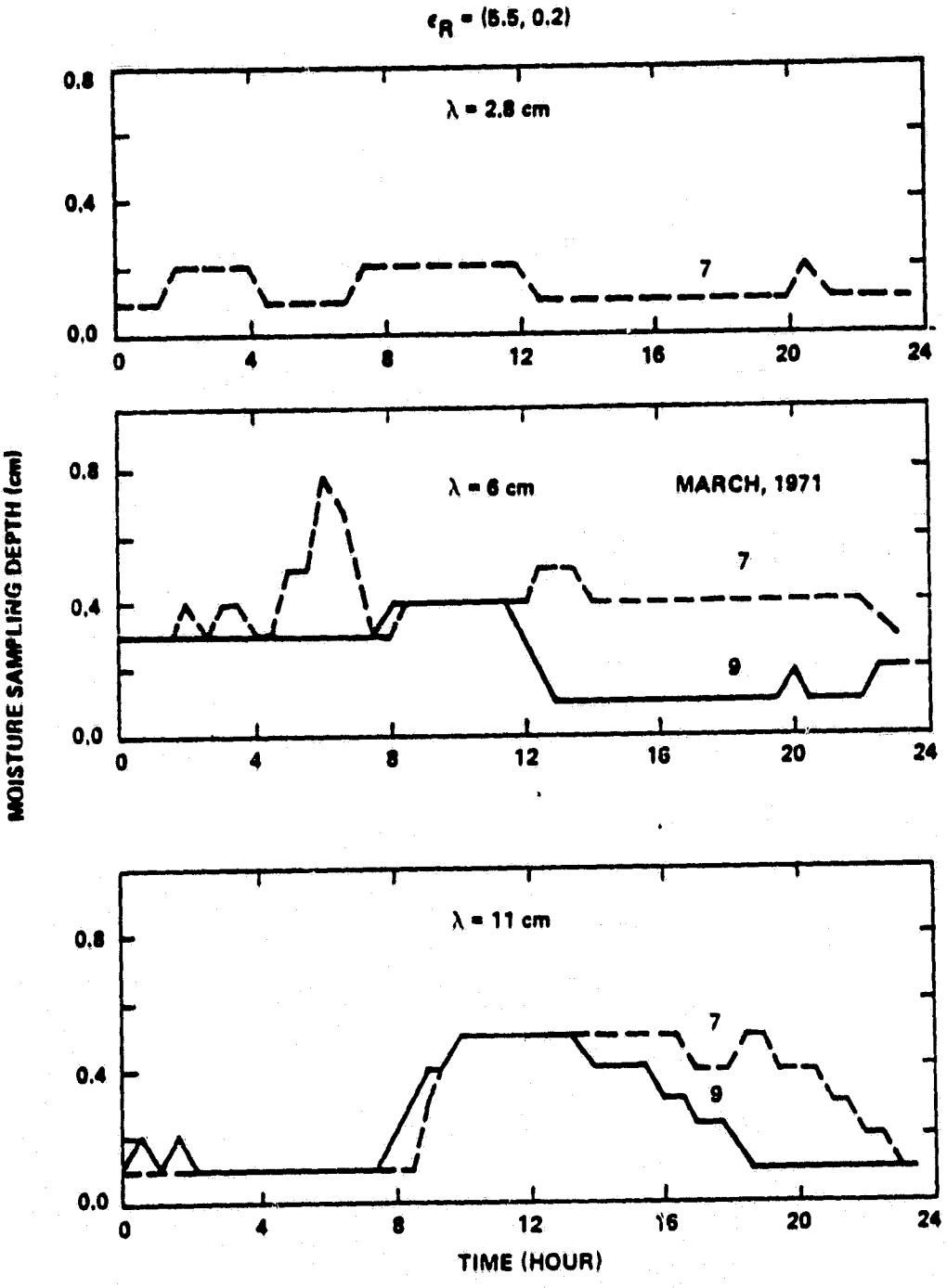

Figure 15. Diurnal variation of the moisture sampling depths at λ = 2.8, 6, and 11 cm. The curves are marked by the days in March 1971 when the Arizona measurements were taken. ϵ_R is the dielectric constant for rock.

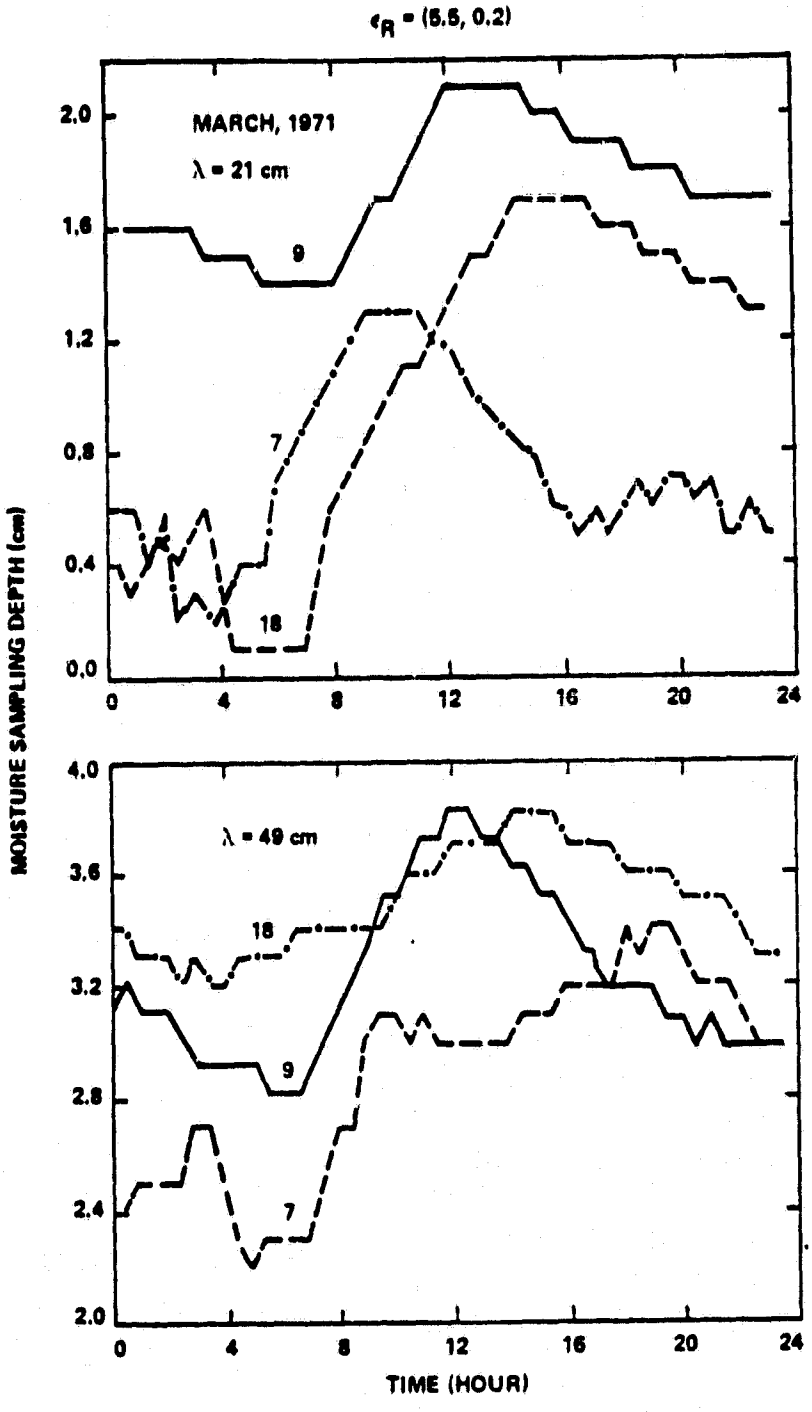

Figure 16. Diurnal variation of the moisture sampling depths at λ = 21 and 49 cm. The curves are marked by the days in March 1971 when the Arizona measurements were taken. ε_R is the dielectric constant of rock.

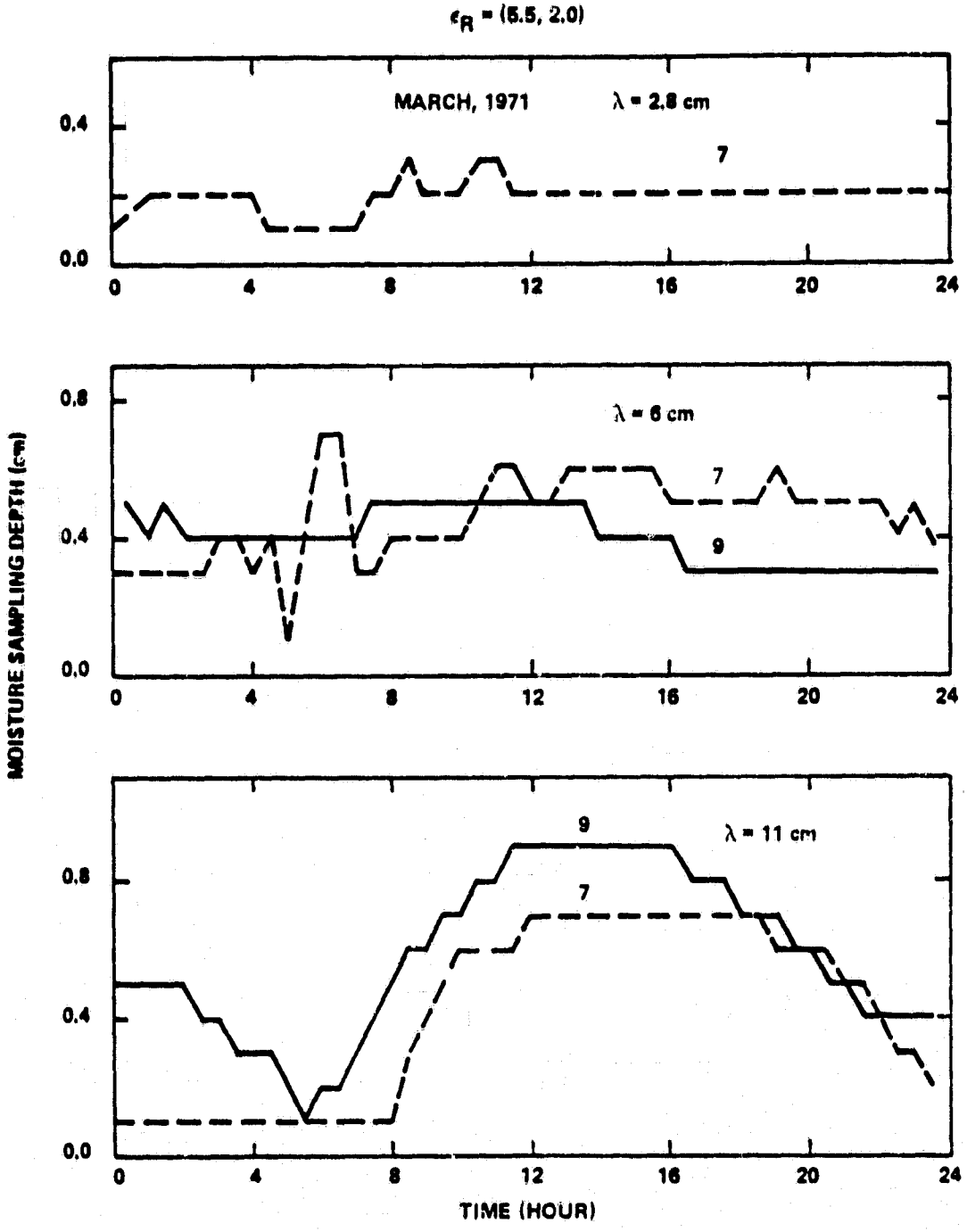

Figure 17. Diurnal variation of the moisture sampling depths at λ = 2.8, 6, and 11 cm. The curves are marked by the days in March 1971 when the Arizona measurements were taken. ε_R is the dielectric constant of rock.

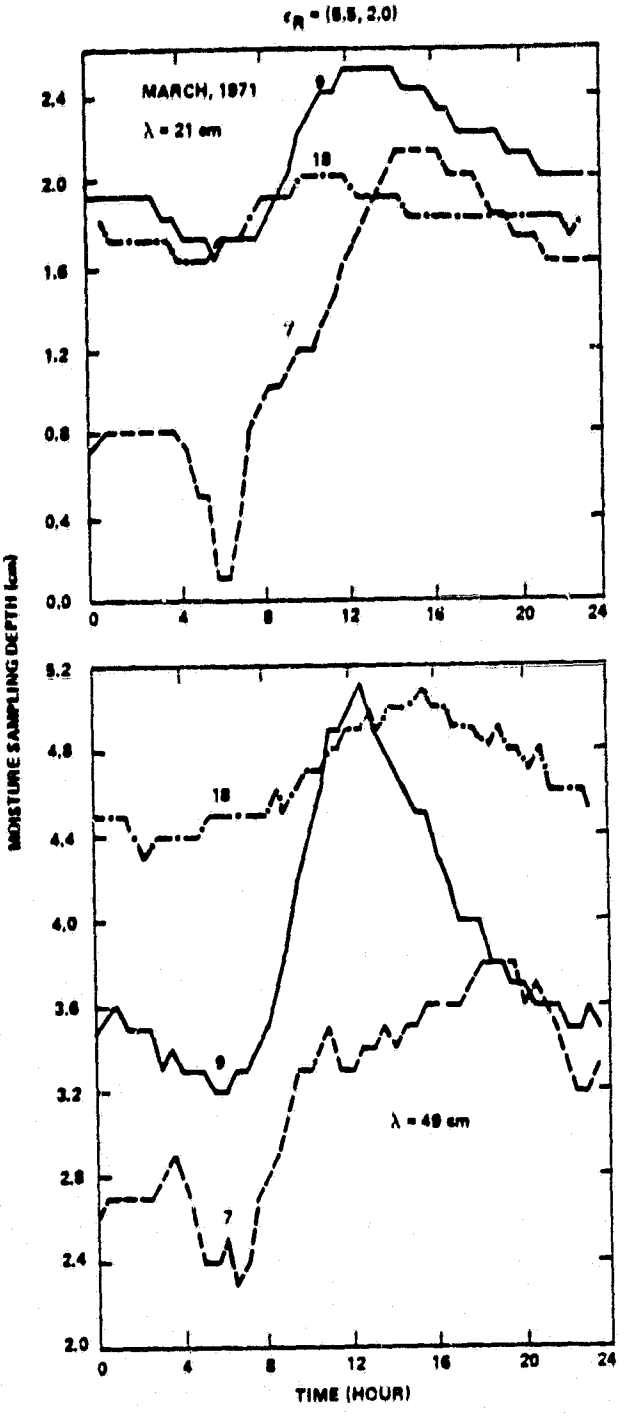

Figure 18. Diurnal variation of the moisture sampling depths at λ = 21 and 49 cm. The curves are marked by the days in March 1971 when the Arizona measurements were taken. ε_R is the dielectric constant of rock.